Available online at www.sciencedirect.com

ScienceDirect

International Journal of Solids and Structures 44 (2007) 4342–4368

INTERNATIONAL JOURNAL OF SOLIDS and STRUCTURES

www.elsevier.com/locate/ijsolstr

Cavity expansion of a gradient-dependent solid cylinder

Jidong Zhao *, Daichao Sheng, Scott W. Sloan

Centre for Geotechnical and Materials Modelling, School of Engineering, The University of Newcastle, NSW 2308, Australia

Received 8 June 2006; received in revised form 2 November 2006; accepted 13 November 2006
Available online 18 November 2006

Abstract

This paper presents an elasto-plastic analysis for cavity expansion in a solid cylinder. The solid is modelled using a strain gradient plasticity model to account for the influence of microstructures on the macroscopic mechanical behaviour. A numerical shooting method, together with Broyden's iteration procedure, is developed to solve the resulting fourth-order ordinary differential equation with two-point boundary conditions for the gradient-dependent problem. Fully elastic-plastic solutions to the cavity expansion are obtained and they are compared with conventional results for a number of examples. The effects of microstructure on macroscopic behaviour for the cavity expansion problem are analysed. It is demonstrated that, with consideration of microstructural effects, the deformation and stress distributions in the cylinder are highly inhomogeneous during both the initial loading and the subsequent elastic and plastic expansion stages. The gradient effects can result in a stiffer response in the elastic regime (as compared with the corresponding conventional prediction), but a weaker response in the plastic regime. As expected, the overall elasto-plastic behaviour of the gradient-dependent cylinder depends on the material parameters as well as the cylinder thickness. It is shown that the strain gradient theory solutions reduce to the conventional ones as a special case when the dimension of the microstructures is negligible compared with the cylinder size. The results in this paper can be used as a benchmark for further numerical investigations of the cavity expansion problem.

Keywords: Solid cylinder; Cavity expansion; Strain gradient plasticity; Microstructure; Numerical shooting method

1. Introduction

The expansion of spherical or cylindrical cavities in finite or infinite media has attracted much attention from researchers in both mechanics and material science. One appealing feature of cavity expansion problems is the simplicity of their geometry, which makes it possible to obtain closed-form solutions for a wide range of applications. Metal indentation tests, for example, have been investigated by Hill (1950) using elasto-plastic cavity expansion theory. A variety of practical geotechnical problems, such as pile installation, cone penetration tests (CPT) and pressuremeter tests (PMT), have also been extensively investigated by cavity expansion analysis (e.g., Gibson and Anderson, 1961). Cavity expansion solutions not only provide valuable predictions

* Corresponding author. Tel.: +61 2 4921 5741; fax: +61 2 4921 6991.
E-mail address: Jidong.zhao@newcastle.edu.au (J. Zhao).

0020-7683/$ - see front matter
doi:10.1016/j.ijsolstr.2006.11.023

for the deformation and pressure-expansion behaviour of these applications, but also furnish benchmarks for comparison with experimental data. Numerous sophisticated constitutive models have been used to obtain cavity expansion solutions which take into account the frictional, cohesive and dilatant behaviour of geomaterials (see e.g., Carter et al., 1986; Yu and Houlsby, 1991; Yu, 1992; Collins et al., 1992; Salgado et al., 1997; Ladanyi and Foriero, 1998). Moreover, cavity expansion theory including both small and large deformations has also been presented (see e.g. Yu (2000) for a review of the topic).

One important feature of geomaterials that has been largely neglected in previous cavity expansion studies is the influence of microstructure. Microstructures exist in many solid materials like soils and rocks in the form of fundamental material grains, microvoids, micro pores and microcracks. Along with the deformation of a material, the microstructural behaviour evolves progressively under load and has a significant influence on the overall macroscopic behaviour of the material. For example, the initial microstructure in a natural soil may cause it to exhibit 'stiffer' mechanical behaviour than the corresponding reconstituted soil (Burland et al., 1996). The neglect of initial microstructure may, therefore, lead to significant discrepancies between observed material behaviour and theoretical predictions from constitutive models. Indeed, conventional continuum theory, on which most existing cavity expansion analyses have been based, does not attempt to address key geomaterial phenomena such as scale effects, strain localisation and catastrophic failure. To resolve these issues, it is now generally accepted that extra terms in the constitutive descriptions are needed to account for microstructural effects. To this end, various high-order theories have been proposed which incorporate gradients of appropriate physical state variables (such as strain or damage), along with one or more intrinsic length scales, in their constitutive formulations. Amongst these strain gradient models, those stemming from generalised Cosserat continua (Cosserat and Cosserat, 1909; Toupin, 1962; Mindlin, 1964, 1965; Germain, 1973) and extended to plasticity theory (Fleck and Hutchinson, 1997), have many potential applications. In strain gradient theory, strain gradients and their work-conjugate forces are considered in addition to the conventional stresses and strains when formulating the constitutive relations. One or more length scales are naturally included when considering the dimension balance for the gradient terms in the governing equations. These length scales represent the influence of microstructure on the macroscopic behaviour of the material. Successful applications of this type of strain gradient theory to practical problems can be found in Zhao et al. (2005, 2007). This paper employs the same theory to re-examine the cavity expansion problem in a solid cylinder, and investigates the effect of microstructure on the deformation-stress and pressure-expansion relations .

There are two major difficulties in applying strain gradient theory to the cylindrical cavity expansion problem. The first is associated with the solvability of the resultant differential governing equations. As will be shown in Section 3, even for the purely elastic model, a fourth-order ordinary differential equation (ODE) with complex boundary conditions needs to be solved for the gradient-dependent case. In this instance, it is difficult to achieve an elegant closed-form analytical solution (as in conventional theory) and we are forced to seek a numerical solution. The finite element method (FEM) has proved to be a powerful tool in many applications and could serve as a good option for the problem. Its key drawbacks for this application, however, are that complex elements with higher-order continuity and delicate plastic flow rules have to be used to accommodate the gradient terms. In view of its axi-symmetric nature, the cylindrical cavity expansion problem can be simplified to a one-dimensional one which can then be solved by other numerical approaches that are simpler than the FEM. In this paper, we employ a numerical shooting approach, together with Broyden's iteration procedure, to solve the governing fourth-order ODE for the elastic regime in the expanding cylinder. To obtain the solution in the plastic regime, the second difficulty arises. For conventional cavity expansion analyses, such as those developed by Hill (1950) and Yu (1992), the plastic regime is assumed to propagate progressively from the inner surface toward the outer surface until it reaches the latter. For the gradient-dependent case to be treated here, this type of plastic expansion behaviour cannot be assumed *a priori*, as inhomogeneous deformations and stresses in the cylinder need to be examined. In our analysis, we first use the purely elastic case to find the point of initial yielding in the cylinder. Assumptions for the subsequent elasto-plastic cavity expansion behaviour are then made and examined using the numerical algorithms developed for the plastic solution.

This paper is organised as follows. Section 2 presents the specific form of strain gradient plasticity model used to study the cylindrical cavity expansion problem. A generalised Tresca yield criterion is proposed to describe the gradient-dependent plastic behaviour in the cylinder. In Section 3, numerical procedures are designed to solve the purely elastic case for the cylindrical expansion. Based on the elastic analysis, the initial

yielding, partly plastic, and fully plastic phases of the problem are then investigated in Section 4. Extensive comparisons between the gradient-dependent solutions and the corresponding conventional ones are made in both Sections 3 and 4. Section 5 gives a summary of the paper and some additional discussions.

2. Constitutive relations and problem description

The solid material is assumed to be homogeneous, isotropic and weightless, with its mechanical behaviour being characterised by a gradient-dependent elastic perfectly-plastic constitutive model. The strain gradient plasticity theory employed here is a generalisation of the linear elasticity strain gradient theory proposed by Toupin (1962), Mindlin (1964, 1965) and Germain (1973) and the extended J_2 plasticity theory of Fleck and Hutchinson (1993, 1997). Whilst finite strain deformation might be more realistic for some applications, the case of small strain deformation is adopted here for the sake of simplicity. Note that it is also possible to extend the subsequent analysis to the case of finite strain, using the formulations presented by Chambon et al. (2004). In addition to the conventional Eulerian strains ε_{ij} and Cauchy stresses σ_{ij}, the strain gradients η_{ijk} and their work-conjugate higher-order stresses τ_{ijk} are also assumed to be present in the material. The strains and strain gradients are, respectively, defined by:

$$\varepsilon_{ij} = \tfrac{1}{2}(u_{i,j} + u_{j,i}), \quad \eta_{ijk} = \tfrac{1}{2}(u_{k,ij} + u_{k,ji}) \tag{1}$$

where both ε_{ij} and η_{ijk} exhibit a symmetry about the indices i and j. Accordingly, the Cauchy stresses σ_{ij} and higher-order stresses τ_{ijk} are also assumed to be symmetric about i and j. Note that in the above, the names of Eulerian strain and Cauchy stress are used merely to distinguish these quantities from the strain gradient and higher-order stress terms. Detailed descriptions of the governing equations and boundary conditions for the strain gradient theory used here can be found in Zhao et al. (2005, 2007), while the corresponding forms in terms of cylindrical coordinates are presented in Appendix A. In what follows, we present only the specific form for the cylindrical cavity expansion problem.

2.1. Cavity expansion in gradient-dependent solid cylinder: problem description

The solid cylinder is assumed to be initially free of stress. From this initial state, the hydrostatic pressure is slowly increased from zero to p_0 throughout the body, as shown in Fig. 1(a). The pressure p_0 is sufficiently small so as not to cause any plastic deformation in the cylinder. As shown in Fig. 1, a cylindrical polar coordinate system (r, θ, z) is adopted, with the hydrostatic pressure p_0 being taken as the initial state for the analysis. From this initial state, the inner surface pressure is gradually increased from p_0 to p, which leads to an interim elastic state as illustrated in Fig. 1(b). This loading process is sufficiently slow so that it may be assumed to be quasi-static. The initial inner and external radii of the cylinder are respectively denoted by a and b and, since small strains are assumed, these values do not change throughout the loading range. At some

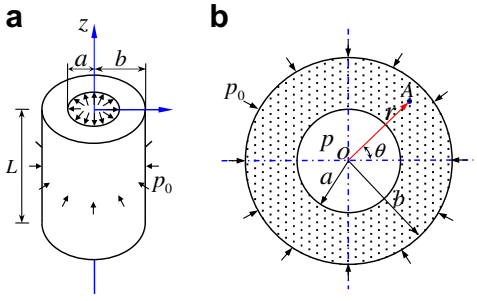

Fig. 1. Illustration of cavity expansion in a gradient-dependent solid cylinder: (a) Initial state with homogeneous hydrostatic pressure p_0 throughout the solid, with the initial radii of the inner cavity wall and exterior wall being denoted by a and b, respectively; (b) An interim elastic state with increased pressure on the inner cavity wall: $p = p_0 + \Delta p$.

interim state, shown in Fig. 1(b), a total increment of pressure $\Delta p = p - p_0$ is supposed to have been applied to the inner cavity wall.

Upon loading, the cylinder first experiences isotropic elastic deformation and then subsequently plastic yielding when the yield condition is met at any point in the cylinder. Initial yielding is said to occur when any point in the cylinder first reaches the plastic state. The corresponding cavity pressure at this stage is called the initial yielding pressure and is denoted by p_{ci}. After this loading stage, the cylinder is supposed to be in a partly plastic state until the entire cylinder body enters the plastic state. The pressure at which the entire body first enters the fully plastic state is called the critical yield pressure, and is denoted by p_{cr}.

2.2. Gradient-dependent constitutive relations in cylindrical coordinates

The length of the cylinder along the z direction, L, is assumed to be much larger than the cylinder thickness, so that generalised plane strain conditions apply and all the components of the strains and strain gradients associated with the z-coordinate are zero. Due to the axi-symmetry of the problem, the displacement u at a point A of the cylinder (see, Fig. 1(b)) can be reasonably assumed to be a function of r only. Consequently, there are only two non-zero strains components, ε_{rr} and $\varepsilon_{\theta\theta}$, and four non-zero strain gradients: η_{rrr}, $\eta_{\theta\theta r}$, $\eta_{r\theta\theta}$, and $\eta_{\theta r\theta}$ where $\eta_{r\theta\theta} = \eta_{\theta r\theta}$. These non-zero components are related to u through the following relations:

$$\varepsilon_{rr} = u_{,r}, \quad \varepsilon_{\theta\theta} = \frac{u}{r}, \qquad \eta_{rrr} = u_{,rr}, \quad \eta_{\theta\theta r} = \frac{1}{r^2}(ru_{,r} - u), \quad \eta_{r\theta\theta} = \eta_{\theta r\theta} = \frac{1}{r}\left(u_{,r} - \frac{u}{2r}\right). \tag{2}$$

A generalised form of Hooke's law first proposed by Mindlin (1965) is used to describe the isotropic linear elastic behavior of the gradient-dependent solid (see also, Zhao et al. (2007), Appendix A there in). Adopting the notation of tension positive, and considering Eq. (2), the following elastic constitutive relations for the conventional and gradient terms are obtained, respectively, as:

$$\begin{cases} \sigma_{rr} = (\lambda + 2\mu)u_{,r} + \frac{\lambda}{r}u \\ \sigma_{\theta\theta} = \lambda u_{,r} + \frac{\lambda+2\mu}{r}u \\ \sigma_{zz} = \lambda\left(u_{,r} + \frac{u}{r}\right) \end{cases} \tag{3}$$

$$\begin{cases} \tau_{rrr} = cl^2\left(5u_{,rr} + \frac{4}{r}u_{,r} - \frac{13}{4r^2}u\right) \\ \tau_{r\theta\theta} = \tau_{\theta r\theta} = cl^2\left(\frac{3}{4}u_{,rr} + \frac{11}{4r}u_{,r} - \frac{7}{4r^2}u\right) \\ \tau_{rzz} = \tau_{zrz} = cl^2\left(\frac{3}{4}u_{,rr} + \frac{3}{4r}u_{,r} - \frac{1}{2r^2}u\right) \\ \tau_{\theta\theta r} = cl^2\left(\frac{3}{2}u_{,rr} + \frac{7}{2r}u_{,r} - \frac{11}{4r^2}u\right) \\ \tau_{zzr} = cl^2\left(\frac{3}{2}u_{,rr} + \frac{3}{2r}u_{,r} - \frac{5}{4r^2}u\right) \end{cases} \tag{4}$$

where λ and μ are the conventional Lamé constants. In these equations, l denotes an internal length scale resulting from the introduction of strain gradients and is related to the dimension of the microstructure in the material. The quantity c denotes a single gradient-dependent elastic parameter, and the five strain gradient combinations $(\eta_{ipp}\delta_{jk} + \eta_{jpp}\ \delta_{ik})$, $(\eta_{ppi}\delta_{jk} + 2\eta_{kpp}\ \delta_{ij} + \eta_{ppj}\delta_{ik})$, $\eta_{ppk}\delta_{ij}$, η_{ijk} and $(\eta_{kji} + \eta_{kij})$ are assumed to be equally important in the determination of the higher-order stress τ_{ijk} (see Mindlin (1965) and Zhao et al., 2007). In the subsequent numerical computations, a value relative to μ will be assigned to the quantity c. The magnitude of this relative value, c/μ, can be used as an index to evaluate the influence of the gradient terms on the overall mechanical behaviour compared to that of the conventional terms.

By neglecting body forces and considering the generalised plane strain condition, Eq. (a.2) of Appendix A gives the following equilibrium equation for the radial direction of the cavity:

$$\frac{\partial\sigma^*_{rr}}{\partial r} + \frac{1}{r}(\sigma^*_{rr} - \sigma^*_{\theta\theta}) = 0 \tag{5}$$

where σ^*_{rr} and $\sigma^*_{\theta\theta}$, respectively, have the following forms:

$$\sigma^*_{rr} = \sigma_{rr} - \left(\frac{\partial\tau_{rrr}}{\partial r} + \frac{1}{r}(\tau_{rrr} - \tau_{\theta\theta r} - \tau_{r\theta\theta})\right) \tag{6}$$

$$\sigma^*_{\theta\theta} = \sigma_{\theta\theta} - \left(\frac{\partial \tau_{\theta r\theta}}{\partial r} + \frac{1}{r}(\tau_{\theta r\theta} + \tau_{r\theta\theta} + \tau_{\theta\theta r})\right) \tag{7}$$

There is also another generalised stress that will be frequently used in the subsequent sections:

$$\sigma^*_{zz} = \sigma_{zz} \tag{8}$$

For the cavity expansion problem, it is readily verified that, in terms of the generalised stresses defined in Eqs. (a.3)–(a.11), only $\sigma^*_{\theta\theta}$, σ^*_{rr} and σ^*_{zz}, are non-zero. In the following, we treat these three stresses as the generalised principal stresses for the analyses.

If the aforementioned three principal stresses satisfy the inequalities $\sigma^*_{\min} \leqslant \sigma^*_{int} \leqslant \sigma^*_{\max}$, the following generalised Tresca criterion is assumed to govern the yield behaviour of the material in the cylinder:

$$f = \sigma^*_{\max} - \sigma^*_{\min} - \kappa = 0 \tag{9}$$

where κ denotes a cohesion parameter of the material. The relative magnitudes of $\sigma^*_{\theta\theta}$, σ^*_{rr} and σ^*_{zz} will be checked in the computations to determine which one corresponds to the maximum or minimum generalised principle stress.

For the cavity expansion problem, the boundary conditions on the inner and outer radii of the cylinder take the following form, respectively:

$$\begin{cases} T_r(a) = \left(-\sigma^*_{rr} + \frac{1}{r}(\tau_{r\theta\theta} - 2\tau_{rrr})\right)\big|_{r=a} = p \\ R_r(a) = \tau_{rrr}|_{r=a} = 0 \end{cases} \tag{10}$$

$$\begin{cases} T_r(b) = \left(\sigma^*_{rr} + \frac{1}{r}\tau_{r\theta\theta}\right)\big|_{r=b} = -p_0 \\ R_r(b) = \tau_{rrr}|_{r=b} = 0 \end{cases} \tag{11}$$

where T and R denote the surface traction and high-order surface traction (see Eqs. (a.12) and (a.13) in Appendix A). Note that the tractability and uniqueness of solution to the above gradient-dependent axi-symmetric boundary values problem can be proved using the procedure proposed by Chambon and Moullet (2004).

3. Gradient-dependent elastic solutions

3.1. Mathematical manipulation of the governing equation

Substitution of Eqs. (6) and (7) into Eq. (5) results in the following equilibrium equation:

$$\frac{\partial \sigma_{rr}}{\partial r} + \frac{\sigma_{rr} - \sigma_{\theta\theta}}{r} - \frac{\partial^2 \tau_{rrr}}{\partial r^2} + \frac{1}{r}\frac{\partial(\tau_{r\theta\theta} + \tau_{\theta r\theta} + \tau_{\theta\theta r} - 2\tau_{rrr})}{\partial r} + \frac{\tau_{r\theta\theta} + \tau_{\theta r\theta} + \tau_{\theta\theta r}}{r^2} = 0 \tag{12}$$

When the stresses at all points in the cylinder satisfy $f < 0$ in Eq. (9), the body is in an elastic state. In this case, one can apply the gradient-dependent elastic relations, Eqs. (3) and (4), to any point in the cylinder. For a point A in an elastic state as shown in Fig. 1(b), the equilibrium equation in the radial direction is obtained by applying Eqs. (3) and (4) to Eq. (12), which leads to the following fourth-order differential equation:

$$\dot{u}_{,rrrr} - \frac{11}{5r}\dot{u}_{,rrr} - \left(\frac{61}{20r^2} + \frac{(\lambda + 2\mu)}{5cl^2}\right)\dot{u}_{,rr} + \left(\frac{51}{20r^3} - \frac{(\lambda + 2\mu)}{5crl^2}\right)\dot{u}_{,r} - \left(\frac{51}{20r^4} - \frac{(\lambda + 2\mu)}{5cr^2l^2}\right)\dot{u} = 0 \tag{13}$$

Eq. (13) and the related boundary conditions, defined by Eqs. (10) and (11), constitute a two-point boundary value problem with a fourth-order homogeneous ordinary differential equation (ODE). It is convenient to re-write the fourth-order homogeneous ODE in Eq. (13) using the following auxiliary variables

$$y_1(r) = \dot{u}, \quad \frac{dy_1}{dr} = y_2(r), \quad \frac{dy_2}{dr} = y_3(r), \quad \frac{dy_3}{dr} = y_4(r) \tag{14}$$

To give the first-order ODE system

$$\frac{\mathrm{d}\mathbf{Y}}{\mathrm{d}r}=\frac{\mathrm{d}}{\mathrm{d}r}\begin{pmatrix}y_1\\ y_2\\ y_3\\ y_4\end{pmatrix}=\begin{pmatrix}y_2\\ y_3\\ y_4\\ g_1y_4+g_2y_3+g_3y_2+g_4y_1\end{pmatrix}=f(\mathbf{Y},r) \tag{15}$$

where: $g_1(r)=\frac{11}{5r}$, $g_2(r)=\frac{61}{20r^2}+\frac{(\lambda+2\mu)}{5cl^2}$, $g_3(r)=-(\frac{51}{20r^3}-\frac{(\lambda+2\mu)}{5crl^2})$ and $g_4(r)=\frac{51}{20r^4}-\frac{(\lambda+2\mu)}{5cr^2l^2}$.

In view of Eqs. (3), (4), (10) and (11), the boundary conditions can now be expressed as:

$$\begin{cases}T_r(a)=\left(5cl^2y_4-\frac{5cl^2}{2r}y_3-((\lambda+2\mu)+\frac{59cl^2}{4r^2})y_2+\left(\frac{25cl^2}{2r^3}-\frac{\lambda}{r}\right)y_1\right)\Big|_{r=a}=p\\ R_r(a)=cl^2\left(5y_3+\frac{4}{r}y_2-\frac{13}{4r^2}y_1\right)\Big|_{r=a}=0\end{cases} \tag{16}$$

$$\begin{cases}T_r(b)=\left(-5cl^2y_4-\frac{6cl^2}{r}y_3+((\lambda+2\mu)+\frac{49cl^2}{4r^2})y_2+\left(\frac{\lambda}{r}-\frac{19cl^2}{2r^3}\right)y_1\right)\Big|_{r=b}=-p_0\\ R_r(b)=cl^2\left(5y_3+\frac{4}{r}y_2-\frac{13}{4r^2}y_1\right)\Big|_{r=b}=0\end{cases} \tag{17}$$

3.2. Numerical solution procedure

Using the procedure proposed by Keller (1968), the existence and uniqueness of a solution to the boundary value problem (BVP) defined by Eqs. (15)–(17) can be easily verified (see also, Chambon and Moullet, 2004; for BVPs with second order gradient models). It is difficult, however, to derive a closed-form solution and some type of numerical method, such as a shooting method or a relaxation technique, is necessary. In this paper we use the shooting method to solve the problem. Such a method first uses an initial estimation for the solution on one boundary to solve the differential equations as a one-point initial value problem. By comparing the computed results with the boundary conditions on the other end, a feedback iteration mechanism is then built to adjust the initial guess on the first end. The whole procedure is then repeated until an accurate solution is found that satisfies both boundary conditions. For a conventional cavity expansion problem, we have verified that a simple shooting method, together with a fourth-order explicit Runge–Kutta approach for solving the ODE (see, e.g., Stoer and Bulirsch, 1980), gives a sufficiently accurate approximation of the exact analytical solution. In the gradient-dependent case, the shooting procedure is more complicated, since there are now two boundary conditions on each face of the cylinder and the simple bisection iteration method is no longer applicable. To overcome this complication, we adopt a version of Broyden iteration during the shooting step, as discussed below.

For a certain pressure level, the shooting method is used to solve the first-order differential equation system (15), subject to the two-point boundary conditions imposed by Eqs. (16) and (17) over the range $r\in[a,b]$. The initial estimation of the solution at one end, as well as the round-off errors generated during the iterations, can greatly influence the accuracy of the results obtained from the shooting method and, in some cases, can even result in divergence of the shooting process. In this paper, we use the analytical solution for the conventional theory to give an initial guess for y_1 and y_2 at $r=a$, so that $y_1=Aa+(B/a)$, and $y_2=A-(B/a^2)$ where A and B are defined in Appendix B. These values are then used to compute the corresponding initial values for y_3 and y_4 at $r=a$ from Eq. (16). The obtained 'initial guess' vector $\mathbf{Y}=(\,y_1\quad y_2\quad y_3\quad y_4\,)^{\mathrm{T}}$ at $r=a$, together with Eq. (15), constitute a one-point initial value problem which is solved by an explicit fourth-order Runge–Kutta approach. To construct the feedback iteration mechanism, the results at the outer boundary $r=b$ are computed and a small perturbation (equal to $\sqrt{eps}$ where *eps* is the machine precision) is applied to the initial guess for $\mathbf{Y}$ at $r=a$ and the one-point boundary value problem is then solved another time. This pair of solutions provides all the necessary components that an iteration procedure needs to adjust the initial values at $r=a$ to make the solution satisfy the boundary conditions at $r=b$. To avoid the complications that may be caused by singularity of the Jacobian matrix in Newton's method, the iteration procedure in this paper is based on Broyden's (Quasi-newton) approach. Moreover, to accelerate the convergence of these iterations, a simple mixing scheme with a coefficient χ is used. As there is no analytical solution available to check the accuracy of the numerical solution, the consistency and stability of the proposed shooting procedure needs to be

carefully examined. The shooting procedure for elastic cavity expansion at a given pressure level is summarised in Appendix C.1.

During conventional cavity expansion, the cylinder will experience three distinct phases of deformation: an elastic stage, a partially plastic stage, and a fully plastic yielding stage. The situation is the same for the gradient-dependent case. As mentioned previously, however, we do not know where and when initial yielding will occur *a priori*, which in turn marks the termination of the elastic computation. Therefore, it is necessary to examine the yield condition for all points in the cylinder during the loading process. Once the yield condition at any point in the cylinder is reached, the expansion enters the initial yielding stage and the elastic solution procedure is stopped. To determine the initial yielding pressure accurately, an appropriate load-stepping procedure needs to be developed. In the first step the hydrostatic pressure is increased throughout the cylinder from zero to p_0 without difficulty, since this stress will not lead to yielding with the generalised Tresca criterion. In the next step, the pressure on the outer wall is kept at p_0, while the pressure on the inner wall is progressively increased. Since isotropic linear elastic relations are employed in the elastic range, we can in theory apply the entire pressure difference $\Delta p = (p_{ci} - p_0)$ in a single step to complete the elastic computation. This cannot be done in practice, however, since the initial yielding pressure p_{ci} is not known *a priori*. To circumvent this problem, we employ the corresponding analytical value from conventional analysis as a rough estimate for p_{ci}. In practice, we avoid applying this load difference Δp in a single step, and divide it into a number of small substeps, e.g., $\Delta p_s = \Delta p/10$. Each time we increase the cavity pressure by Δp_s and solve the problem by the shooting procedure outlined above. Upon obtaining the solution for each load step, the yield condition is checked for each point in the cylinder. Eventually, the initial yielding stage is passed and the corresponding load step 'overshoots' the solution in the sense that more than one point in the radial direction of the cylinder enters a plastic state (the number of points characterising the cylinder depends on a solver tolerance that will be specified). In this case, a bisection procedure has been designed to reduce the load step to the exact pressure that causes initial yielding and is summarised in Appendix C.2.

3.3. Numerical results and discussions

The above algorithms have been implemented in a MATLAB (Ver. 6.5) code. It is convenient to use the explicit Runge–Kutta routine ODE45 in the MATLAB package to solve the initial value problems in Steps 5 and 11 of the shooting procedure (Appendix C.1). Using this code, the elastic solutions for the gradient-dependent cavity expansion problem are investigated. In the subsequent computations, we choose the following parameters for the elastic analysis of the cavity expansion:

$$a = 1.0, \quad \frac{b}{a} = 2.0, \quad \frac{\lambda}{\mu} = 2.0, \quad \frac{p_0}{\mu} = 0.2, \quad \frac{\Delta p_s}{p_0} = 0.1, \quad \frac{c}{\mu} = 1.0, \quad \frac{l}{a} = 0.1, \quad \frac{\kappa}{p_0} = 3.0.$$

Note that, except at the inner cavity radius a, all the parameters are assumed to be dimensionless. The relative error and absolute error for the ODE45 solution are controlled to a prescribed tolerance TOL, which at the same time controls the number of the radial points in the cylinder. The smaller TOL is set, the more points there are in the solution. In the Broyden iteration procedure, the perturbation to the initial guess of $\mathbf{Y}_a$ is set to be $\sqrt{eps}$ times its current value. For the computer used in the simulations $\sqrt{eps} = 1.4901E-8$. The performance of the Broyden iteration procedure is also controlled by the specified tolerance TOL (as shown in Step 18 in the shooting algorithm, Appendix C.1).

3.3.1. Consistency and stability study

To examine the consistency and stability of the proposed solution procedure, various tolerances were specified with TOL chosen to be 10^{-2}, 10^{-4}, 10^{-6}, 10^{-7}, 10^{-8} and 10^{-10}. The computational results for the relative displacements (u/a) at $r = a$ and $r = b$ are presented in Table 1 (at a pressure level of $p/p_0 = 1.25$ under which the cylinder is still in a purely elastic state). The relative errors of u/a at various tolerances, with respect to the "reference" values for $TOL = 10^{-10}$, are also computed. As expected, the solutions obtained converge to the reference values in a stable and consistent manner as the prescribed tolerance is tightened. Indeed, once the prescribed tolerance is smaller than about 10^{-8}, the solution for the problem is identical to that with $TOL = 10^{-10}$. Besides the above examination of the tolerance effects, we also tried different initial guesses

Table 1
Consistency of the numerical algorithm to specified tolerance

TOL	Inner surface displacement ($r = a$)		Exterior surface displacement ($r = b$)	
	$(u/a)\|_{r=a}$	Relative error (%)	$(u/a)\|_{r=b}$	Relative error (%)
10^{-2}	−0.0090291299	7.42*e*−E5	−0.2375814956	6.25*e*−E3
10^{-4}	−0.0090291226	6.65*e*−E6	−0.2375665146	6.08*e*−E5
10^{-6}	−0.0090291233	1.11*e*−E6	−0.2375666585	2.10*e*−E7
10^{-7}	−0.0090291232	0	−0.2375666592	8.42*e*−E8
10^{-8}	−0.0090291232	0	−0.2375666590	0
10^{-10}	−0.0090291232	–	−0.2375666590	–

for y_1 and y_2 at $r = a$ to test the stability of the proposed algorithms. Arbitrary values ranging over $[-1000, 1000]$ for both y_1 and y_2 were employed, and no divergence was detected. The solutions obtained for these cases were consistent with those found by initialising y_1 and y_2 to the corresponding conventional results (as suggested in the algorithms). Nevertheless, we observed that the latter values generally gave much faster convergence than the rest. In view of the above, the proposed algorithms appear to give stable and consistent solutions. In all subsequent analyses, the tolerance is fixed at a value of $TOL = 10^{-10}$.

3.3.2. Stress distributions in the cylinder at the hydrostatic pressure p_0

In this part, the stress distribution in the cylinder is investigated for the initial loading state where the hydrostatic pressure is increased from zero to p_0. The Cauchy stresses and generalised principal stresses in the cylinder for the gradient-dependent case are plotted against those for the conventional case in Fig. 2. For convenience, we hereafter denote the results computed from conventional theory by the term 'conventional theory results', while those obtained using the strain gradient theory will be denoted by the term 'gradient theory results'. As depicted in Fig. 2, the conventional results for both σ_{rr} and $\sigma_{\theta\theta}$ are homogeneous throughout the cylinder for the initial state of uniform hydrostatic pressure, whereas the gradient theory values are not. The gradient-dependent stresses σ_{rr} and $\sigma_{\theta\theta}$ are both slightly larger in absolute magnitude than the corresponding conventional ones in the vicinity of the inner wall, but are slightly smaller near the outer wall. Nevertheless, the discrepancy between the two distributions is quite small, with the largest difference for σ_{rr} and $\sigma_{\theta\theta}$ being 0.76% and 0.99%, respectively. The distributions for the generalised principal stresses, $\sigma^*_{\theta\theta}$ and σ^*_{rr}, are also shown in Fig. 2 by dotted lines. These quantities are not homogeneous across the cylinder section either.

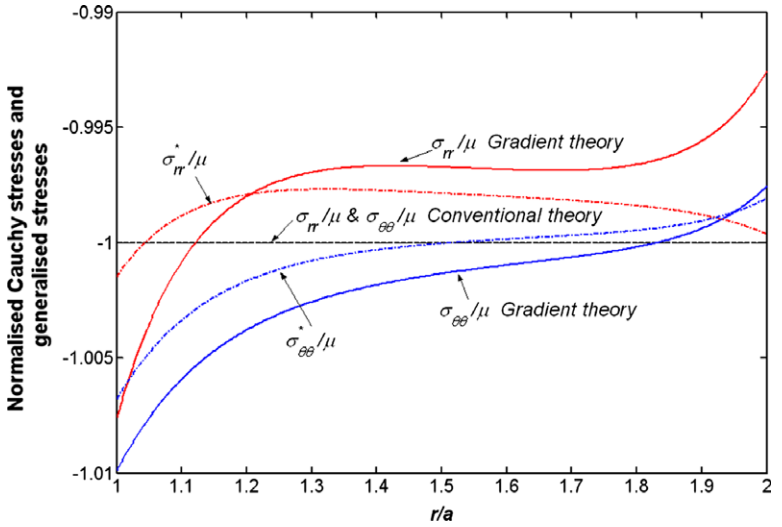

Fig. 2. Normalized conventional stresses, normalized Cauchy stresses and normalized generalized principal stresses in gradient-dependent solid cylinder under a homogeneous hydrostatic pressure p_0.

To account for the higher-order stress terms, the distribution of σ^*_{rr} is slightly flattened between the conventional curve for σ_{rr} and the corresponding gradient-dependent one. Similar behaviour is observed for the distribution of $\sigma^*_{\theta\theta}$. The absolute magnitude of σ_{zz} is much smaller than either σ_{rr} or $\sigma_{\theta\theta}$ at this pressure level, and is not shown here.

3.3.3. Parametric sensitivity study ($p/p_0 = 1.25$)

It is interesting to investigate the sensitivity of the model response to some of the key parameters. We choose an expansion pressure of $p/p_0 = 1.25$, at which the cylinder is found to be still in a purely elastic state. The parameters chosen for the study are the ratio of the high-order elastic modulus to the conventional one c/μ and the internal length scale ratio l/a. Keeping l/a at 0.1, we first chose six groups of c/μ for the study: $c/\mu = 0$, 0.2, 1, 2, 4 and 10. It is noted that a smaller value of c/μ implies the gradient effects are weaker compared with the conventional behaviour, and vice versa. The obtained results are presented in Fig. 3.

From Fig. 3(a) we see that larger values of c/μ lead to the gradient stress distribution σ_{rr} being above the conventional one. When c/μ is as smaller than about 0.2, the gradient theory stress distribution is very close to that the conventional one, except in the vicinity of the inner wall. As expected, when $c/\mu = 0$, the gradient-dependent curve for σ_{rr} is identical to the conventional one. The influence of c/μ on the stresses τ_{rrr} and $\tau_{\theta\theta r}$ is more pronounced, as shown in Figs. 3(b) and (c), respectively. When $c/\mu = 0$, the gradient effects vanish and both τ_{rrr} and $\tau_{\theta\theta r}$ are identically zero across the cylinder radius, so that the conventional results are immediately recovered. The strain gradient theory may thus be viewed as a more general framework which includes the conventional theory as a special case.

The influence of the internal length scale on the mechanical response was studied using six different length scales: $l/a = 0$, 0.05, 0.08, 0.1, 0.2, and 0.5. The normalised stresses σ_{rr} and τ_{rrr} for these cases are shown in Figs. 4(a) and (b), respectively. Compared with its conventional counterpart, the gradient-dependent stress σ_{rr} is always larger and the difference increases with increasing l/a. As expected, when l/a is quite small (less than about 0.05), there is little disparity between the two distributions. In a like manner, larger values of l/a change the response for τ_{rrr} dramatically, with this component vanishing for $l/a = 0$. When the length scale is small compared to the dimension of the problem, the microstructural influence is negligible and the conventional theory is expected to give similar results to the gradient theory. When this scale is comparable to the problem size, however, the effects of microstructures will become significant and large differences in the response may be expected.

3.3.4. Variation of deformations and stresses in the cylinder at $p/p_0 = 2$

Using the same parameters as in the beginning of Section 3.3, we now investigate the stress and deformation distributions when the cavity pressure is at a higher level of $p/p_0 = 2.0$. No yielding occurs at this pressure, and the distributions shown in Figs. 5 and 6 are still in the elastic range.

Fig. 5 depicts the radial displacement and its gradients obtained from both the conventional theory and gradient theory. The gradient-dependent curves for the displacement and its gradients lie below the corresponding conventional ones, with the largest differences between the three variables all occurring at the inner wall of the cavity. For purely elastic cavity expansion with the current choice of model parameters, the introduction of the gradient terms thus leads to a slightly stiffer response for the material.

At this pressure level, a further investigation of the normalised Cauchy stresses, generalised stresses and higher-order stresses is presented in Fig. 6. From Fig. 6(a) we see that, at this pressure, the magnitudes of the gradient-dependent σ_{zz} and $\sigma_{\theta\theta}$ are slightly smaller than those from conventional theory. As forσ_{rr}, the gradient-dependent results are smaller than the corresponding conventional ones over the inner half of the radius, but become greater in the outer half. This figure also shows the generalised stress $\sigma^*_{\theta\theta}$ is quite close to the gradient-dependent stress $\sigma_{\theta\theta}$, but smaller than the conventional one. The generalized stress σ^*_{zz} is identical with the gradient-dependent quantity σ_{zz}. Fig. 6(b) shows that τ_{rrr} is the largest high-order stress at any point in the cylinder, with the stresses $\tau_{\theta\theta r}$, $\tau_{r\theta\theta}$ and $\tau_{\theta r\theta}$ being substantially smaller than the other ones. The high-order stresses τ_{rrr}, τ_{zzr}, τ_{rzz} and τ_{zrz} all reach a peak near the inner wall, while $\tau_{\theta\theta r}$, $\tau_{r\theta\theta}$ and $\tau_{\theta r\theta}$ have a monotonically increasing distribution with a maximum value at the outer wall. τ_{rrr} vanishes at both the inner and outer radii due to the high-order boundary conditions imposed by Eqs. (16) and (17).

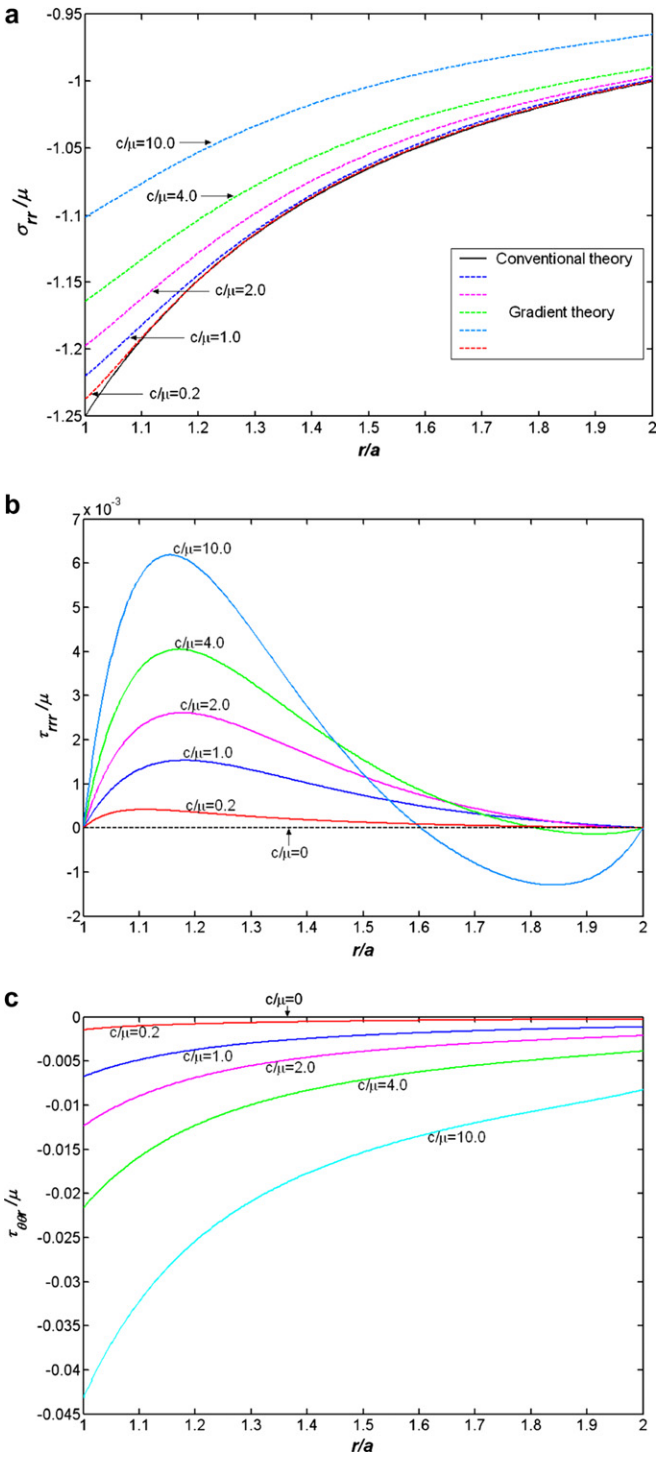

Fig. 3. Sensitivity of normalized Cauchy stresses and higher stresses to c/μ at $p/p_0 = 1.25$. (a) Normalised stress σ_{rr} across the cylinder wall as a function of c/μ. (b) Normalised τ_{rrr} across the cylinder wall as a function of c/μ. (c) Normalised $\tau_{\theta\theta r}$ across the cylinder wall as a function of c/μ.

It is of particular interest to see from Fig. 6(a) that, under the current cavity pressure, σ^*_{zz} is the intermediate generalised principal stress, with $\sigma^*_{\theta\theta}$ and σ^*_{rr} being, respectively, the maximum and minimum ones. During the computations at other pressure levels in the elastic range, it was also found that the maximum value for

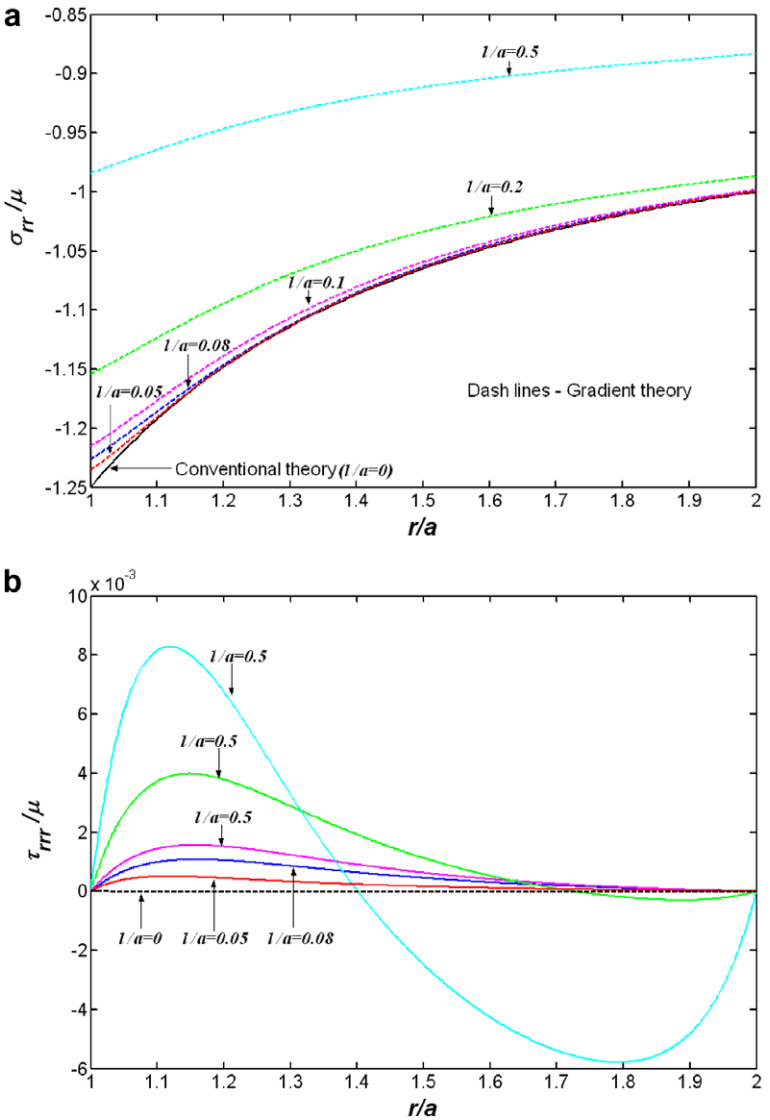

Fig. 4. Sensitivity of normalized σ_{rr} and τ_{rrr} to l/a at $p/p_0 = 1.25$. (a) Normalised σ_{rr} across the cylinder wall as a function of l/a. (b) Normalised τ_{rrr} across the cylinder wall as a function of l/a.

$K = (\sigma^*_{\max} - \sigma^*_{\min})$ always occur at the inner cavity wall. Therefore, the initial yielding will occur first at this surface. We also investigated the development of the three generalised principal stresses at $r = a$ during various elastic loading levels. The results, shown in Fig. 7, reveal that σ^*_{zz} is not always the intermediate generalised principal stress as we have expected. During the initial hydrostatic loading stage the compressive stresses $\sigma^*_{\theta\theta}$ and σ^*_{rr} increase proportionally from zero, with σ^*_{zz} being the maximum one. When the inner expansion pressure begins to increase, σ^*_{rr} increases at the same rate, while $\sigma^*_{\theta\theta}$ and σ^*_{zz} reduce in their compressive value. Prior to the cavity pressure reaching $p = 0.13\mu$, σ^*_{zz} is the maximum principal stress and σ^*_{rr} is the minimum principal stress. Once this pressure level is exceeded, σ^*_{zz} becomes the intermediate principal stress and $\sigma^*_{\theta\theta}$ is the maximum principal stress. This behaviour is maintained until initial yielding occurs. Therefore, when the pressure level is large enough ($p/\mu > 0.13$ for this case), it is safe to use the following yield function in place of Eq. (9):

$$\sigma^*_{\theta\theta} - \sigma^*_{rr} = \kappa \tag{18}$$

In practical applications, the displacement at the outer surface is a convenient quantity to measure. Fig. 8 shows the pressure-expansion curve during elastic cavity expansion in terms of the displacement at the outer

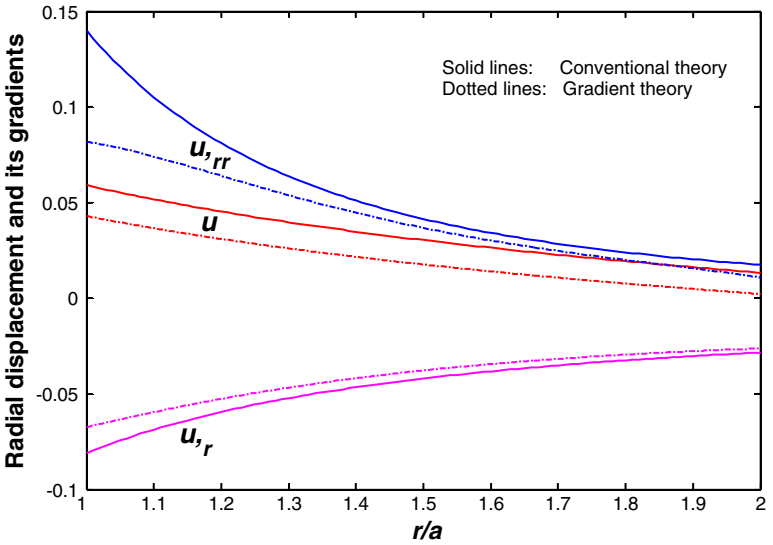

Fig. 5. Comparison between conventional and gradient-dependent radial displacement and its gradients across the cylinder radius ($p/p_0 = 2$).

wall. The conventional results are also depicted in comparison. As can be seen from the figure, during the initial hydrostatic loading stage, the exterior cylinder wall is compressively deformed and thus moves inwards. When the cavity pressure is increased from the initial state, the overall deformation is still in compression; however, when the pressure is high enough, the exterior cylinder wall begins to move outwards. The elastic gradient-dependent curve again exhibits a 'stiffer' response than the conventional one.

4. Gradient-dependent plastic solutions

According to the preceding analyses for the purely elastic case, we may conclude that: (1) when the cavity pressure is large enough, the maximum and minimum generalised stresses are $\sigma^*_{\theta\theta}$ and σ^*_{rr}, respectively; and (2) initial yielding occurs at the inner cavity surface. At this stage, we cannot predict the behaviour under loading beyond initial yielding; nevertheless, we will make some assumptions which we will examine *a posteriori*. In analogue to the conventional case it is assumed that, upon further loading, yielding will develop from the inner wall and spread outwards to the exterior wall in a progressive manner. At any intermediate state of this process, the solid cylinder is said to be *partly plastic*. Once the plastic zone reaches the exterior surface, collapse occurs and the cylinder is *fully plastic*.

In this section, we investigate the initial yielding behaviour and then seek the partly plastic and fully plastic solutions. We will restrict the plastic analysis of cavity expansion at the point a fully plastic state is first entered in the cylinder. Once entering the fully plastic state, the solid will experience unlimited plastic flow at a constant rate as dictated by the elasto-perfectly-plastic flow rule. In the partly plastic case, we suppose the outer extent of the plastic zone is defined by the radius ρ, which lies between the inner and outer walls of the cylinder (Fig. 9).

4.1. Theoretical investigation of the plastic expansion behaviour

4.1.1. Initial yielding

Using the condition that initial yielding occurs at the inner cavity surface, we can accurately compute the initial yielding pressure p_{ci} as defined before. Upon initial yielding, the cylinder is still in an elastic state except at the inner cavity surface. Hence we can still use the numerical shooting method, presented in Section 3, to

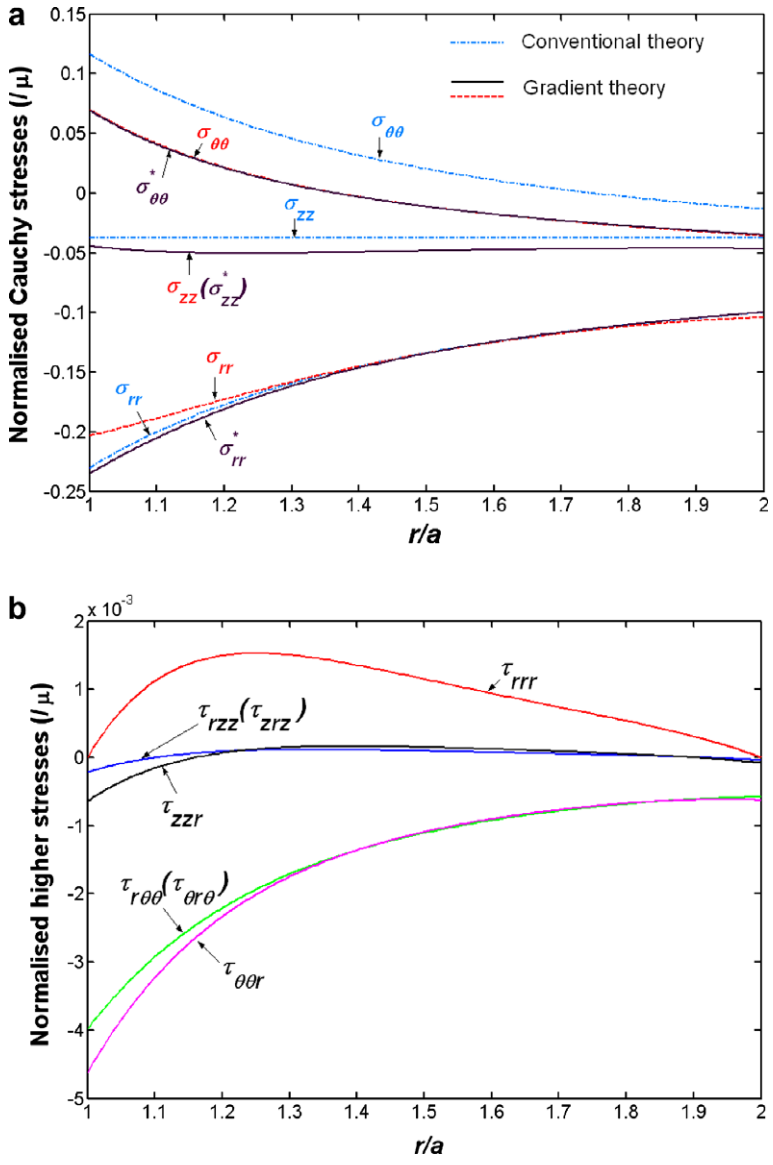

Fig. 6. Variation of normalised Cauchy stresses, generalised stresses and high-order stresses across the cylinder for $p/p_0 = 2$. (a) Normalised Cauchy stresses and generalised stresses. (b) Normalised high-order stresses.

solve the problem. The only difference now is that the boundary conditions at the inner cavity wall are changed to:

$$\begin{cases} (\sigma^*_{\theta\theta} - \sigma^*_{rr})\big|_{r=a} = \kappa \\ \tau_{rrr}|_{r=a} = 0 \end{cases} \tag{19}$$

The first equation denotes the yielding condition at $r = a$, while the second one defines the high-order traction at $r = a$. Substituting the elastic relations (3) and (4) into (19), and using Eq. (14), we obtain the left boundary conditions for the numerical shooting procedure. The right boundary conditions at $r = b$ remain the same as those presented in Eq. (17). Hence, the ODE presented in Eq. (15), together with these two new end boundary conditions, is now solvable by the shooting method presented in Section 3.2 and the displacement and stress

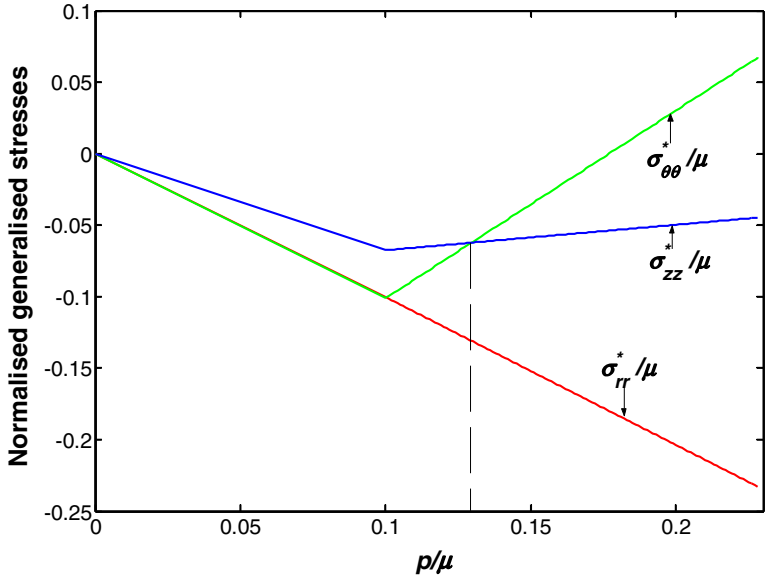

Fig. 7. Normalised generalised stresses at $r = a_0$ for various cavity pressures (elastic solution).

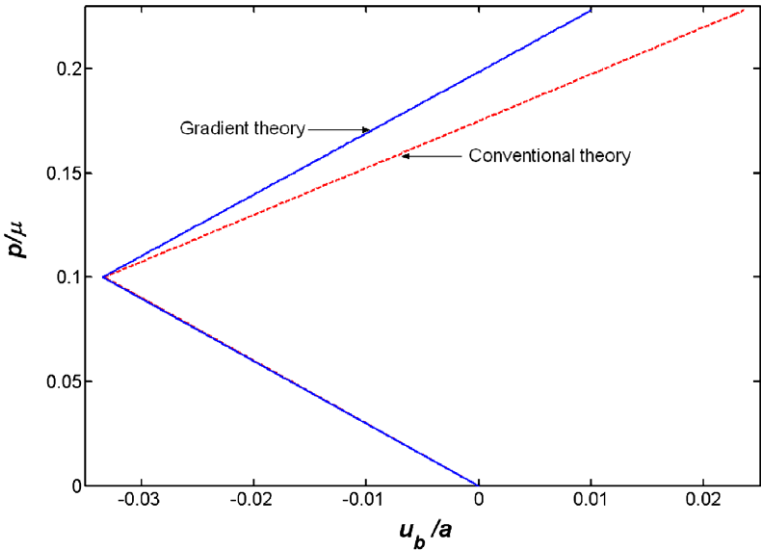

Fig. 8. Pressure-expansion curve for exterior wall of the cylinder during elastic loading.

field in the cylinder can be completely determined. On determining the stress field, the initial yielding pressure can also be obtained by the traction condition at $r = a$:

$$p_{\mathrm{ci}} = T_r(a) = \left[-\sigma_{rr} + \tau_{rrr,r} - \frac{1}{r}(\tau_{rrr} + \tau_{\theta\theta r})\right]\Big|_{r=a} = \left[-\sigma^*_{rr} + \frac{1}{r}\tau_{r\theta\theta}\right]\Big|_{r=a} \tag{20}$$

where the high-order traction condition $\tau_{rrr}|_{r=a} = 0$ has been used. Note that the pressure p_{ci} so obtained can be used to check the results of the previous purely elastic stage.

4.1.2. Partly plastic solutions

The solution procedures for the partly and fully plastically deformed cylinder are complicated. In conventional mechanics, the assumptions of small strain and a Tresca yield criterion render the stress field in the

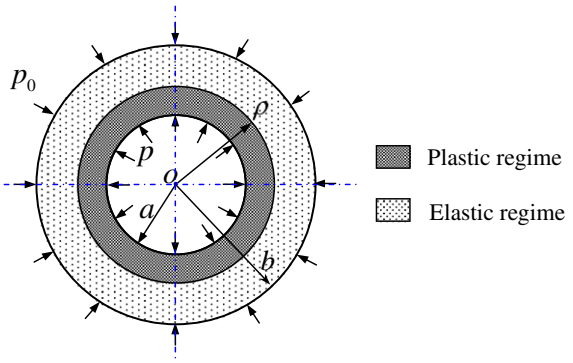

Fig. 9. Partly plastic deformation for cavity expansion in a gradient-dependent solid cylinder.

cylinder statically determinate, and it is possible to derive the Cauchy stresses merely by knowing ρ and the cavity pressure p without needing to calculate the deformation in the plastic region (e.g., Hill, 1950). For the Mohr-Coulomb criterion, Yu (1992) found the partly plastic solution after computing the deformation field in the plastic region first. For the gradient-dependent model treated here, the problem is too complicated to be analytically solvable, even though we have assumed small strains and a simple generalisation of the Tresca yield criterion. The key difficulty is that the stress field in the plastic region is not statically determinate because of the number of unknown state variables and the nature of the boundary conditions. As a result, we are unable to derive a relation between the stresses, the plastic boundary ρ, and the cavity pressure p. Moreover, the deformation in the plastic region cannot be easily obtained due to the intricate plastic flow rules that have to be assumed for both the plastic strain rates and plastic strain gradient rates. Some form of numerical procedure is the only option, and this is described below.

As shown in the previous section, it is appropriate to use $\sigma^*_{\theta\theta}$ and σ^*_{rr} as the maximum and minimum generalised principal stresses, respectively, provided the cavity is still in an elastic state. When yielding occurs, we further assume that $\sigma^*_{\theta\theta}$ and σ^*_{rr} remain the two extreme generalised stresses in the plastic region $a \leqslant r < \rho$. This implies that Eq. (18) still governs. In view of Eqs. (11) and (18), the following relation is thus assumed to hold in the plastic regime:

$$\frac{\partial \sigma^*_{rr}}{\partial r} = \frac{\sigma^*_{\theta\theta} - \sigma^*_{rr}}{r} = \frac{\kappa}{r} \tag{21}$$

The boundary conditions for the plastic regime at $r = a$ remain the same as those in the elastic state

$$\begin{cases} T_r(a) = -\sigma^*_{rr} + \frac{1}{r}\tau_{r\theta\theta}\big|_{r=a} = p \\ R_r(a) = \tau_{rrr}|_{r=a} = 0 \end{cases} \tag{22}$$

while the boundary conditions for the plastic regime at $r = \rho$ need to satisfy the continuity conditions for the stresses and high-order stresses. It is noted that ρ and p are not independent of each other so that, given a plastic regime radius ρ, the corresponding cavity pressure p should be determined. To this end, we seek the solution to the elastic regime over the domain $\rho \leqslant r \leqslant b$ first, and assume that the plastic boundary ρ increases progressively from a to b. In the following, ρ is taken as known before solving the entire problem, and the current plastic radius is denoted as ρ_i, where the subscript i denotes the *ith* incremental step for ρ with $\rho_1 = a$.

To solve the ODE (15) for the displacements in the elastic regime we need two boundary conditions at $r = \rho_i$. We have already another two at $r = b$, defined by Eqs. (17), that are identical to the purely elastic case. We now focus on seeking the boundary conditions at $r = \rho_i$. These two boundary conditions should be expressed without any explicit reference to the cavity pressure p. The yield condition and the governing equations for the stresses at $r = \rho_i$ are as follows:

$$\begin{cases} \sigma^*_{\theta\theta} - \sigma^*_{rr} = \kappa \\ \frac{\partial \sigma^*_{rr}}{\partial r} = \frac{\sigma^*_{\theta\theta} - \sigma^*_{rr}}{r} = \frac{\kappa}{r} \end{cases} \tag{23}$$

Note that similar conditions have also be stated by Chambon et al. (1998, 2001) for localisation studies of geomaterials with second gradient theories. After substituting the elastic relations in Eqs. (3) and (4), and inserting Eqs. (6) and (7) into the above conditions, and using the substitutions (14), we obtain the following expressions for the elastic regime at $r = \rho_i$:

$$\begin{cases} \frac{17}{4}cl^2 y_4 + \frac{cl^2}{r}y_3 - \left(\frac{14cl^2}{r^2} + 2\mu\right)y_2 + \left(\frac{2\mu}{r} + \frac{21cl^2}{2r^3}\right)y_1\Big|_{r=\rho} = \kappa \\ -\frac{3}{4}cl^2\frac{\mathrm{d}y_4}{\mathrm{d}r} - \frac{23}{4r}cl^2 y_4 + \left(\lambda + \frac{5cl^2}{4r^2}\right)y_3 + \left(\frac{\lambda+2\mu}{r} + \frac{47cl^2}{4r^3}\right)y_2 - \left(\frac{\lambda+2\mu}{r^2} + \frac{33cl^2}{4r^4}\right)y_1\Big|_{r=\rho} = \frac{\kappa}{\rho} \end{cases} \tag{24}$$

The numerical shooting procedure described in Section 3 works by first making an initial guess for y_1 and y_2, and then solving for y_3 and y_4 from the boundary conditions at $r = a$. For this partly plastic case, we need to start the shooting process at $r = \rho_i$. However, there is an extra unknown term, $\mathrm{d}y_4/\mathrm{d}r$, in the second equation of Eq. (24), which prevents us from solving for y_3 and y_4, even if we have initial estimates for y_1 and y_2 at $r = \rho_i$. To seek and approximate value for $\mathrm{d}y_4/\mathrm{d}r$, we first assume that the incremental step for ρ is sufficiently small, such that the value of $\mathrm{d}y_4/\mathrm{d}r$ can be estimated from the previous incremental step. Using the last equation in the ODE system in Eq. (15) we obtain:

$$\varphi_{i-1} = \left.\frac{\mathrm{d}y_4}{\mathrm{d}r}\right|_{\rho_i} = (g_1 y_4 + g_2 y_3 + g_3 y_2 + g_4 y_1)|_{\rho_{i-1}} \tag{25}$$

where ρ_{i-1} and ρ_i are, respectively, the last and current plastic regime boundary radii. Substituting Eq. (25) into (24) and combining the initial guess for y_1 and y_2 at $r = \rho_i$, we can then solve for y_3 and y_4 at $r = \rho_i$. On obtaining y_1 to y_4 at $r = \rho_i$, the numerical shooting procedure as presented in Section 3 can then be used to compute the solution for the elastic regime. This solution is an approximate one, as the value for $\mathrm{d}y_4/\mathrm{d}r$ was estimated from the previous step. To compute a more accurate solution, the values $\tilde{y}_1$, $\tilde{y}_2$, $\tilde{y}_3$ and $\tilde{y}_4$ at $r = \rho_i$ are re-substituted into the last equation in Eq. (15) to give a new value for $\mathrm{d}y_4/\mathrm{d}r$:

$$\tilde{\varphi}_i = \left.\frac{\mathrm{d}y_4}{\mathrm{d}r}\right|_{\rho_i} = (g_1\tilde{y}_4 + g_2\tilde{y}_3 + g_3\tilde{y}_2 + g_4\tilde{y}_1)|_{\rho_i} \tag{26}$$

This process is then repeated until the difference between two successive iterations for $\tilde{\varphi}_i$ becomes sufficient small. The final solution is then taken as the solution for the elastic regime $\rho_i \leqslant r \leqslant b$.

Upon obtaining the elastic regime solution, we can find $\sigma_{rr}^{*(\rho)}$ and $\sigma_{\theta\theta}^{*(\rho)}$ at $r = \rho_i$ for the plastic regime by using the stress continuity conditions at $r = \rho_i$. Using Eq. (21) this gives:

$$\frac{\sigma_{rr}^{*(\rho_i)} - \sigma_{rr}^{*}}{\kappa} = \ln\frac{\rho_i}{r}, \quad \frac{\sigma_{\theta\theta}^{*} - \sigma_{rr}^{*(\rho_i)}}{\kappa} = \ln\frac{\rho_i}{r} - 1 \tag{27}$$

Letting $r = a$ we obtain the generalised stresses at the inner surface as:

$$\sigma_{rr}^{*(a)} = \sigma_{rr}^{*(\rho_i)} - \kappa\ln\frac{\rho_i}{a}, \quad \sigma_{\theta\theta}^{*(a)} = \kappa\left(\ln\frac{\rho_i}{a} - 1\right) + \sigma_{rr}^{*(\rho_i)} \tag{28}$$

Now the traction boundary condition at $r = a$ is:

$$\left(-\sigma_{rr}^{*} + \frac{1}{r}\tau_{r\theta\theta}\right)\Big|_{r=a} = p \tag{29}$$

The value of σ_{rr}^{*} at $r = a$ can be calculated from Eq. (28), but we cannot derive the value of $\tau_{r\theta\theta}$ directly, which prevents us from evaluating the cavity pressure from Eq. (29). The value of $\tau_{r\theta\theta}$ at $r = a$, however, can be estimated approximately using the analysis of Section 4.1, which shows that σ_{rr}^{*} and $\tau_{r\theta\theta}$ at initial yielding can be obtained analytically. Numerical computations show that, compared to σ_{rr}^{*}, $\tau_{r\theta\theta}$ is very small and is therefore not significant in calculating the cavity pressure from Eq. (29). Nevertheless, since we can obtain the value of $\tau_{r\theta\theta}$ at $r = a$ for the initial yielding state, we will use this value of $\tau_{r\theta\theta}$ but assume that it does not vary significantly during the partly and fully plastic loading stages. Using this approach will give a better approximation for p than one obtained by totally neglecting the effects of $\tau_{r\theta\theta}$ in Eq. (29). Therefore, the cavity pressure during the partly plastic stage is assumed to be:

$$p \cong -\sigma_{rr}^{*(a)} + \frac{1}{a}\hat{\tau}_{r\theta\theta}^{(a)} \tag{30}$$

where $\hat{\tau}_{r\theta\theta}^{(a)}$ denotes the value of $\tau_{r\theta\theta}$ at $r = a$ for the initial yielding state. Note that the above approximation only affects the predicted cavity pressure.

To determine the displacements in the plastic regimes, additional assumptions regarding the plastic flow rule are required. The implications of these assumptions are beyond the scope of this paper, and will not be pursued here. We therefore do not intend to investigate the deformation behaviour in the plastic regime. Since we can derive the cavity pressure-outer wall displacement curve, as well as the generalised stress distributions in the cylinder, these results will be sufficient for the comparison with conventional results.

4.1.3. Fully plastic state

When ρ_i reaches a value of b the plastic zone has reached the outer boundary and the cylinder is said to be in a fully plastic state. In this case, the numerical shooting procedure will be no longer appropriate as the computational domain is now zero. Nevertheless, for any point on the outer surface of the cylinder at the critical cavity pressure p_{cr}, the elastic relations still apply and the stresses must satisfy the yield condition. Therefore, there are now four equations for any point on the outer surface: two from Eq. (17) and two from Eq. (23). Using the value for dy_4/dr from the previous incremental step as an initial guess, the displacements at the outer surface can be analytically determined. The values for y_1 to y_4 so obtained can then be substituted into the last equation in Eq. (15) to obtain another value for dy_4/dr. This process can then be repeated until dy_4/dr remains constant within a prescribed tolerance. The final results for y_1 to y_4 give the displacement and its gradients at the outer surface, and the stresses and higher-order stresses can then be determined using the elastic relations (3) and (4). Employing Eqs. (28)–(30), the generalised stresses and cavity pressure for the onset of fully plastic flow can also be obtained.

4.2. Numerical results and discussions

We now summarise the plastic solution procedures for cavity expansion outlined in Section 4.1 and present them in terms of a numerical algorithm in Appendix C.3. This algorithm is then used to predict the expansion of a gradient-dependent cavity in the plastic range. The same example as in the elastic case will be considered. The number of increments used for the development of the plastic regime, N_ρ, is set to 100 but numerical experience suggests that the results are somewhat insensitive to this value. Larger increments cause an increase in the iterations, though the final solutions are approximately the same.

4.2.1. Variation in generalised principal stresses during plastic expansion

Fig. 10 illustrates the variation in the normalised stresses σ_{rr}^* and $\sigma_{\theta\theta}^*$ across the cylinder wall as a function of the plastic radiusρ. The conventional results for σ_{rr} and $\sigma_{\theta\theta}$ are also presented in the figures for comparison, and data are given for the five steps where $\rho/a = 1$, 1.25, 1.5, 1.75 and 2. In Figs. 10(a) and (b), the conventional elastic results are denoted by green dashes lines, with the plastic results being shown by black dashed lines. The gradient-dependent elastic and plastic results for σ_{rr}^* are indicated by solid blue and red lines, respectively.

Fig. 10(a) shows that the elastic and plastic curves for σ_{rr}^* are smoothly continuous at the plastic regime boundary ρ and, before the fully plastic stage is reached, are smaller than the corresponding conventional stress σ_{rr} at any point of the cylinder. At the onset of fully plastic deformation, however, σ_{rr}^* is slightly larger than σ_{rr}. Fig. 10(b) shows that the stress $\sigma_{\theta\theta}^*$ in the elastic and plastic regimes is still continuous at the plastic radius ρ but nonsmooth. This mirrors the behaviour from conventional theory for $\sigma_{\theta\theta}$. It is also evident that, prior to the onset of any plastic deformation, the generalised stress $\sigma_{\theta\theta}^*$ is always smaller than its conventional counterpart $\sigma_{\theta\theta}$. At the onset of fully plastic deformation, however, $\sigma_{\theta\theta}^*$ and the conventional stress $\sigma_{\theta\theta}$ are quite similar, with $\sigma_{\theta\theta}^*$ being slightly greater than $\sigma_{\theta\theta}$.

As an *a posteriori* check, we also investigated the relative magnitudes of $\sigma_{\theta\theta}^*$, σ_{rr}^* and σ_{zz}^* during various stages of plastic expansion. Typical results for the generalised principal stresses in the plastic regime, shown in Fig. 11, indicate that during all stages of plastic expansion σ_{zz}^* remains the intermediate stress of the three,

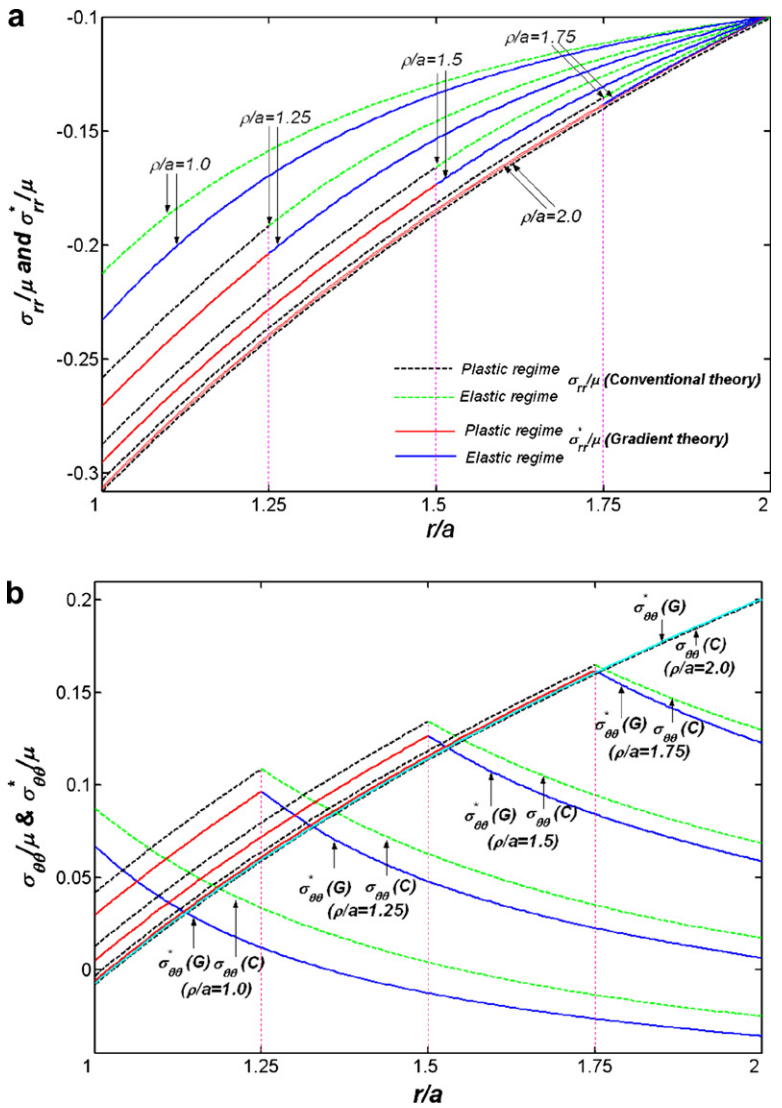

Fig. 10. Variations of the normalized stresses σ^*_{rr} and $\sigma^*_{\theta\theta}$ as a function of the plastic radius. ('G' denotes gradient theory; 'C' denotes conventional theory). (a) Variation of normalized stress σ^*_{rr} as a function of the plastic radius. (b) Variation of the normalized stress $\sigma^*_{\theta\theta}$ as a function of the plastic radius. (For interpretation of the references to color in this figure legend, the reader is referred to the web version of this paper.)

while $\sigma^*_{\theta\theta}$ is the maximum. This confirms the validity of the yield criterion assumption presented in Eq. (18). Fig. 11. also shows that the difference $(\sigma^*_{\theta\theta} - \sigma^*_{rr})$, for the elastic regime in the cylinder, is always a maximum value at the elastic–plastic interface. This implies that, whenever further plastic yielding occurs, it always happens at this interface so that the plastic regime will develop in a progressive manner from the inner cavity radius to the outer cavity radius. This matches the assumptions made *a priori* in the analysis.

4.2.2. Parametric sensitivity study

It is interesting to investigate the plastic pressure-displacement relation in terms of the cavity pressure and the displacement at the outer surface (the response during the elastic loading period is linear). Fig. 12 shows several such plots for various choices of the parameter c/μ, as well as the plot for conventional cavity expansion theory ($c/\mu = 0$). Compared with the conventional curve, the gradient-dependent $p - u$ responses are generally stiffer but have a slightly lower ultimate pressure at the fully plastic state. For example, the ultimate

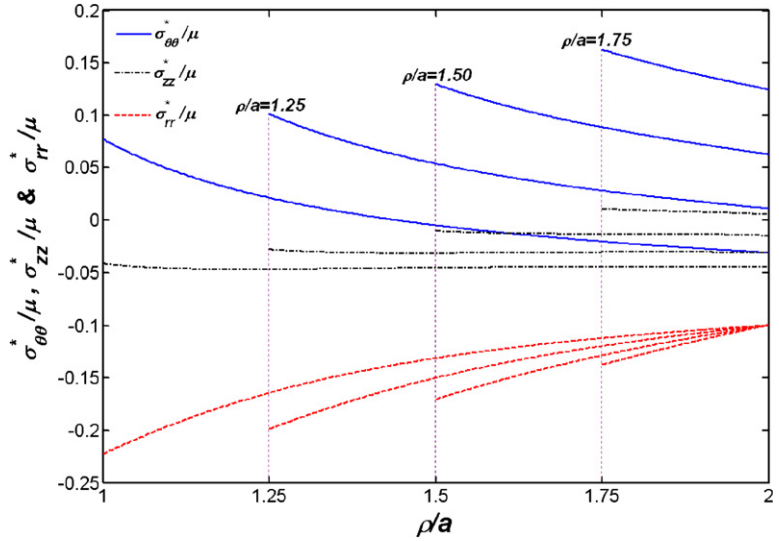

Fig. 11. Normalized plastic stresses for a gradient-dependent solid at different values of ρ/a.

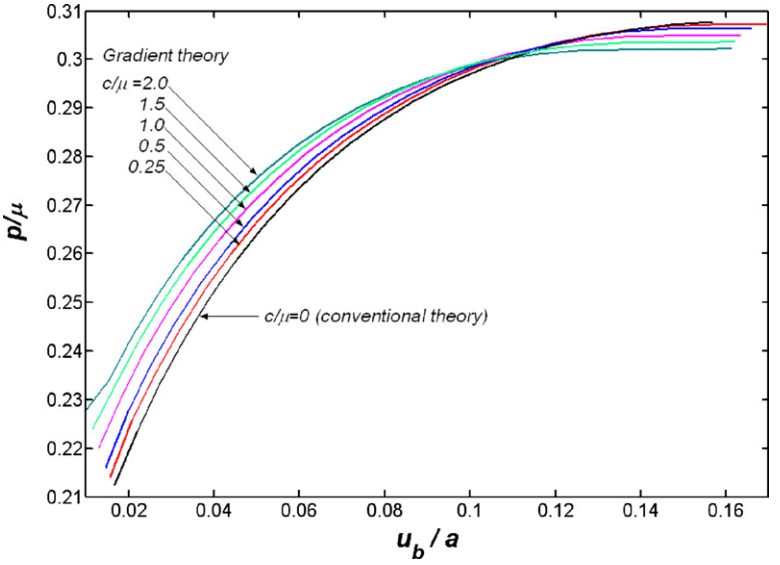

Fig. 12. Pressure-expansion relation for plastic loading of a gradient-dependent solid at different values of c/μ ($l/a = 0.1$).

pressure difference at the fully plastic state for $c/\mu = 0.25$ is 0.24% and 0.93% for $c/\mu = 2$. Since smaller value of c/μ imply that the effects of the gradient terms are less significant, these results are as expected.

Fig. 13 shows the pressure-expansion response when we fix c/μ at 1 and vary the internal length scales according to: $l/a = 0.05$, 0.075, 0.1, 0.125 and 0.15. The gradient-dependent pressure-expansion curves are again stiffer than the conventional response, but exhibit a slightly lower ultimate collapse pressure. As expected, the predicted $p - u$ relations are closer to the conventional curve for small values of l/a, where the dimension of the microstructure is small in relation to the problem size. In the extreme case of $l/a = 0$, which corresponds to a material whose microstructural size is negligible in comparison with the problem size, the gradient effects can be totally disregarded and the conventional results are immediately recovered.

The results in Section 3 suggest that the gradient-dependent material gives a stiffer response than a conventional one in the elastic range. This additional stiffness carries over into the partly plastic stage of cavity

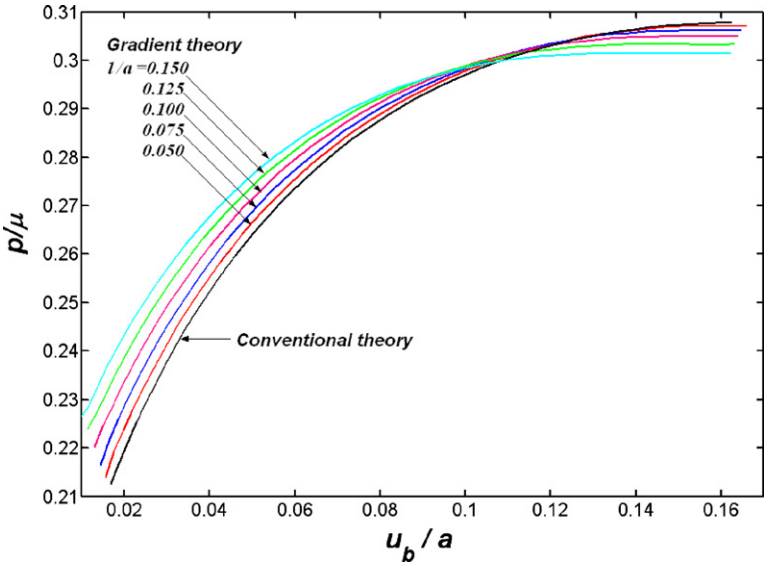

Fig. 13. Pressure-expansion relation for a cavity expansion in a gradient-dependent solid at different values of l/a ($c/\mu = 1.0$).

expansion, prior to the onset of plastic collapse. The effect of the gradient terms on the overall elasto-plastic response, as expected, is significantly influenced by the cylinder thickness. In connection with Figs. 12 and 13, when the cylinder is relative thin ($b/a = 2$), the stiffening effects in the elastic region outweigh the weakening effects in the plastic regime during most of the loading process, so that most of the gradient-dependent p–u curve is above the conventional one until the critical cavity pressure is approached. During the computations we also found that the expansion pressure p and the elastic-plastic radius ρ are almost linearly related. Therefore, for a thin cylinder, the stiffening effects from the elastic region are still significant up until 95% or so of the cylinder has entered the plastic state. For a thick cylinder the situation is quite different. To illustrate this point, we also investigated the pressure-expansion responses for three other cases with $b/a = 4$, 6 and 10. To make the gradient effects discernable for these examples, the corresponding internal length scales were increased to $l/a = 0.2$, 0.3 and 0.4. The quantity c/μ was fixed at 1, and the other parameters were unchanged from the previous computations.

The results, presented in Fig. 14, show that the pressure-expansion responses for the different cases are generally similar in shape, but have widely varying collapse pressures. As expected, the thicker cylinders have the highest ultimate cavity pressures. As the cylinder thickness increases, the elastic stiffening effect caused by the gradient-dependent terms becomes less pronounced. This is to say, in a thick cylinder, the stiffening effects from the elastic region decay more quickly than in a thin cylinder. For example, for the case of $b/a = 10$, the weakening effects in the plastic region outweigh the stiffening effects from the elastic region when 1/7 of the cylinder is still elastic. In contrast, for the case of $b/a = 2$, this transition occurs when only a small elastic area is left in the cylinder ($\rho \approx b/30$). This phenomenon can be interpreted as a size effect for the cylindrical expansion problem, and is only discernable by the use of gradient theory.

Fig. 14 also shows that for thick cylinders with $b/a > 2.0$, the outer wall initially experiences compressive deformation and moves inwards. This implies that, initially, this surface does not feel the effects of the cavity pressure and is mainly deformed by the hydrostatic pressure imposed on the outer wall.

5. Summary and discussions

This paper has investigated cylindrical cavity expansion in elasto-plastic gradient-dependent media. The strain gradient plasticity model assumes small strains and is used in combination with a generalised form of Tresca's yield criterion. A numerical shooting method and Broyden's iteration procedure are used to solve the governing fourth-order ODE equation system with two-point boundary conditions. The elastic and plastic

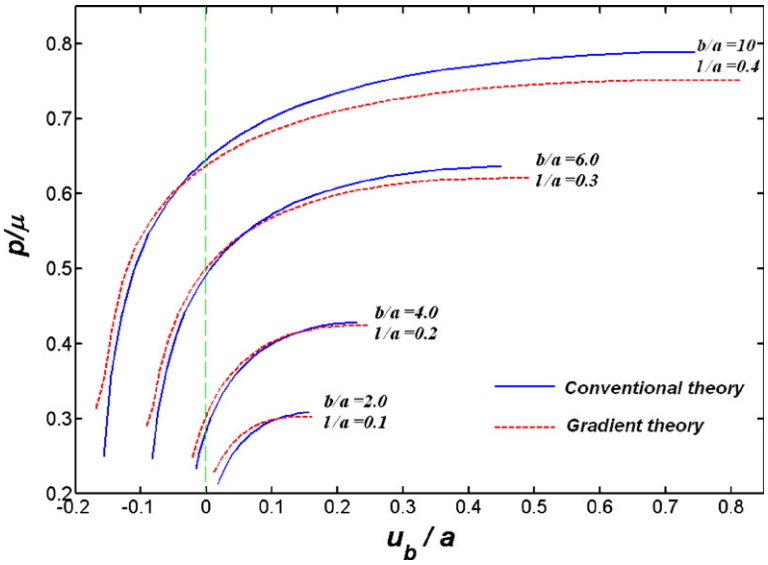

Fig. 14. Pressure–expansion relations for gradient-dependent solid cylinders of varying thickness.

solutions obtained have been compared extensively against those derived from conventional analysis. Major conclusions from the analysis are:

(1) The numerical shooting procedures are effective in dealing with the gradient-dependent governing equations. The results obtained are generally insensitive to the prescribed tolerance and initial values assumed for the problem.
(2) The stress distribution in the cylinder for the gradient-dependent case is highly inhomogeneous, even under a uniform hydrostatic pressure at the initial state.
(3) The influence of microstructure on the stress and deformation during the cavity expansion process can be modelled by adjusting the gradient-dependent elastic modulus and the internal length scale. When these quantities are large, the cavity expansion solutions exhibit pronounced differences from those obtained by conventional theory.
(4) The gradient-dependent material generally has a stiffer elastic response than a conventional material under cavity expansion, but displays a weaker response in the plastic regime. During the elasto-plastic expansion, the combined effects from the elastic and plastic regions of the cylinder cause a transition point in the response. Before this point the stiffening effects from the elastic regime dominate, while after it the weakening effects from the plastic regime prevail.
(5) For a thin cylinder, the stiffening effects from the elastic region are evident until the cylinder is about to enter the fully plastic state; whereas for a thick cylinder, the stiffening effects are dissipated much earlier in the loading process when a relatively large fraction of the cylinder is still in an elastic state. This size effect for the cavity expansion problem stems from the nature of the gradient-dependent model used in the analysis.

It is worth noting that the proposed numerical procedure for solving the gradient-dependent cavity expansion problem cannot be used to simulate the case of cavity expanding from a zero radius via a similarity solution. This is because all the length variables in the present analysis have been normalised with respect to the inner cavity radius. Moreover, the strains in this instance are large (see, e.g., Collins et al., 1992). To deal with the situation of a cavity expanding from a zero radius, the cylinder thickness could be used as a reference for the normalisation. To consider the case of an infinite cylinder width, the average material grain size could be used as a reference length. However, this may result in the gradient effects being negligible if the internal length scale is too small compared with the problem dimension. Moreover, the current solution to the plastic

expansion case is not a closed form one, as the deformation in the plastic regime has not been obtained. To compute these deformations, additional plastic flow rules involving gradient terms need to be considered. We also note that the present strain gradient formulation could be generalised to a finite strain form, e.g., according to the approach proposed by Chambon et al. (2004). This would allow large strain examples, such as pile installation, to be analysed more rigorously.

Where possible, it is preferable for theoretical studies to be benchmarked against experimental data. This is not done in the present work because, in contrast to various conventional theories, gradient-enhanced theories have so far received relatively little calibration against real data due to their recent development. Indeed, many of their parameters are still an open question. Nevertheless, we suggest that the semi-analytical solutions for cavity expansion in a higher order continuum presented here can be used for benchmarking of any similar studies in the future.

Appendix A. Strain gradient theory in cylindrical coordinates

In Zhao et al. (2005, 2007), the strain gradient theory was presented in a general tensor form using rectangular coordinates. For the cavity expansion problem, however, alternative formulations in cylindrical coordinates need to be developed. The translation between the two coordinates for the strain gradient theory, though conceptually simple, is not straightforward as it involves intricate tensor manipulations. We have derived formulations for elastic strain gradient theory in orthogonal curvilinear coordinates (Zhao and Sheng, 2006), according to the procedure as suggested by Eringen (1967) for conventional mechanics. Here the results for cylindrical coordinates, and the simplification for the cavity expansion problem, are provided. The following gradient-dependent equilibrium equations hold for cylindrical coordinates:

$$\begin{cases} \dfrac{\partial \sigma^*_{rr}}{\partial r} + \dfrac{1}{r}\dfrac{\partial \sigma^*_{\theta r}}{\partial \theta} + \dfrac{\partial \sigma^*_{zr}}{\partial z} + \dfrac{1}{r}(\sigma^*_{rr} - \sigma^*_{\theta\theta}) = 0 \\ \dfrac{\partial \sigma^*_{r\theta}}{\partial r} + \dfrac{1}{r}\dfrac{\partial \sigma^*_{\theta\theta}}{\partial \theta} + \dfrac{\partial \sigma^*_{z\theta}}{\partial z} + \dfrac{1}{r}(\sigma^*_{r\theta} + \sigma^*_{\theta r}) = 0 \\ \dfrac{\partial \sigma^*_{rz}}{\partial r} + \dfrac{1}{r}\dfrac{\partial \sigma^*_{\theta z}}{\partial \theta} + \dfrac{\partial \sigma^*_{zz}}{\partial z} + \dfrac{1}{r}\sigma^*_{rz} = 0 \end{cases} \tag{a.1}$$

where

$$\sigma^*_{rr} = \sigma_{rr} - \left(\frac{\partial \tau_{rrr}}{\partial r} + \frac{1}{r}\frac{\partial \tau_{r\theta r}}{\partial \theta} + \frac{\partial \tau_{rzr}}{\partial z} + \frac{1}{r}(\tau_{rrr} - \tau_{\theta\theta r} - \tau_{r\theta\theta})\right)$$

$$\sigma^*_{\theta\theta} = \sigma_{\theta\theta} - \left(\frac{\partial \tau_{\theta r\theta}}{\partial r} + \frac{1}{r}\frac{\partial \tau_{\theta\theta\theta}}{\partial \theta} + \frac{\partial \tau_{\theta z\theta}}{\partial z} + \frac{1}{r}(\tau_{\theta r\theta} + \tau_{r\theta\theta} + \tau_{\theta\theta r})\right)$$

$$\sigma^*_{zz} = \sigma_{zz} - \left(\frac{\partial \tau_{zrz}}{\partial r} + \frac{1}{r}\frac{\partial \tau_{z\theta z}}{\partial \theta} + \frac{\partial \tau_{zzz}}{\partial z} + \frac{1}{r}\tau_{zrz}\right)$$

$$\sigma^*_{\theta r} = \sigma_{\theta r} - \left(\frac{\partial \tau_{\theta rr}}{\partial r} + \frac{1}{r}\frac{\partial \tau_{\theta\theta r}}{\partial \theta} + \frac{\partial \tau_{\theta zr}}{\partial z} + \frac{1}{r}(\tau_{\theta rr} + \tau_{r\theta r} - \tau_{\theta\theta\theta})\right)$$

$$\sigma^*_{r\theta} = \sigma_{r\theta} - \left(\frac{\partial \tau_{rr\theta}}{\partial r} + \frac{1}{r}\frac{\partial \tau_{\theta r\theta}}{\partial \theta} + \frac{\partial \tau_{zr\theta}}{\partial z} + \frac{1}{r}(\tau_{rr\theta} + \tau_{r\theta r} - \tau_{\theta\theta\theta})\right)$$

$$\sigma^*_{zr} = \sigma_{zr} - \left(\frac{\partial \tau_{zrr}}{\partial r} + \frac{1}{r}\frac{\partial \tau_{z\theta r}}{\partial \theta} + \frac{\partial \tau_{zzr}}{\partial z} + \frac{1}{r}(\tau_{zrr} - \tau_{z\theta\theta})\right)$$

$$\sigma^*_{rz} = \sigma_{rz} - \left(\frac{\partial \tau_{rrz}}{\partial r} + \frac{1}{r}\frac{\partial \tau_{\theta rz}}{\partial \theta} + \frac{\partial \tau_{zrz}}{\partial z} + \frac{1}{r}(\tau_{rrz} - \tau_{\theta\theta z})\right)$$

$$\sigma^*_{\theta z} = \sigma_{\theta z} - \left(\frac{\partial \tau_{r\theta z}}{\partial r} + \frac{1}{r}\frac{\partial \tau_{\theta\theta z}}{\partial \theta} + \frac{\partial \tau_{z\theta z}}{\partial z} + \frac{1}{r}(\tau_{r\theta z} + \tau_{\theta rz})\right)$$

$$\sigma^*_{z\theta} = \sigma_{z\theta} - \left(\frac{\partial \tau_{zr\theta}}{\partial r} + \frac{1}{r}\frac{\partial \tau_{\theta z\theta}}{\partial \theta} + \frac{\partial \tau_{zz\theta}}{\partial z} + \frac{1}{r}(\tau_{rz\theta} + \tau_{zr\theta})\right)$$

For the special case of the cavity expansion problem treated here, a generalised plane strain state is assumed where the displacement associated with the z axis vanishes. In addition, the problem is axi-symmetric so that all the variables are independent of θ. In view of this, all the partial differential terms with respect to z and θ in Eq. (11) can thus be dropped, which leads to the following equilibrium equations for the cavity expansion problem:

$$\begin{cases} \frac{\partial \sigma^*_{rr}}{\partial r} + \frac{1}{r}(\sigma^*_{rr} - \sigma^*_{\theta\theta}) = 0 \\ \frac{\partial \sigma^*_{r\theta}}{\partial r} + \frac{1}{r}(\sigma^*_{r\theta} + \sigma^*_{\theta r}) = 0 \\ \frac{\partial \sigma^*_{rz}}{\partial r} + \frac{1}{r}\sigma^*_{rz} = 0 \end{cases} \tag{a.2}$$

where

$$\sigma^*_{rr} = \sigma_{rr} - \left(\frac{\partial \tau_{rrr}}{\partial r} + \frac{1}{r}(\tau_{rrr} - \tau_{\theta\theta r} - \tau_{r\theta\theta})\right) \tag{a.3}$$

$$\sigma^*_{\theta\theta} = \sigma_{\theta\theta} - \left(\frac{\partial \tau_{\theta r\theta}}{\partial r} + \frac{1}{r}(\tau_{\theta r\theta} + \tau_{r\theta\theta} + \tau_{\theta\theta r})\right) \tag{a.4}$$

$$\sigma^*_{\theta r} = \sigma_{\theta r} - \left(\frac{\partial \tau_{\theta rr}}{\partial r} + \frac{1}{r}(\tau_{\theta rr} + \tau_{r\theta r} - \tau_{\theta\theta\theta})\right) \tag{a.5}$$

$$\sigma^*_{r\theta} = \sigma_{r\theta} - \left(\frac{\partial \tau_{rr\theta}}{\partial r} + \frac{1}{r}(\tau_{rr\theta} + \tau_{r\theta r} - \tau_{\theta\theta\theta})\right) \tag{a.6}$$

$$\sigma^*_{rz} = \sigma_{rz} - \left(\frac{\partial \tau_{rrz}}{\partial r} + \frac{1}{r}(\tau_{rrz} - \tau_{\theta\theta z})\right) \tag{a.7}$$

We also have the following generalised stresses which do not appear in the equilibrium equations:

$$\sigma^*_{zz} = \sigma_{zz} - \left(\frac{\partial \tau_{zrz}}{\partial r} + \frac{1}{r}\tau_{zrz}\right) \tag{a.8}$$

$$\sigma^*_{zr} = \sigma_{zr} - \left(\frac{\partial \tau_{zrr}}{\partial r} + \frac{1}{r}(\tau_{zrr} - \tau_{z\theta\theta})\right) \tag{a.9}$$

$$\sigma^*_{\theta z} = \sigma_{\theta z} - \left(\frac{\partial \tau_{r\theta z}}{\partial r} + \frac{1}{r}(\tau_{r\theta z} + \tau_{\theta rz})\right) \tag{a.10}$$

$$\sigma^*_{z\theta} = \sigma_{z\theta} - \left(\frac{\partial \tau_{zr\theta}}{\partial r} + \frac{1}{r}(\tau_{rz\theta} + \tau_{zr\theta})\right) \tag{a.11}$$

The traction and higher-order traction conditions for the inner and outer cavity faces read:

$$\begin{cases} T_r(a) = (-\sigma^*_{rr} + \frac{1}{r}(\tau_{r\theta\theta} - 2\tau_{rrr}))\big|_{r=a} = p \\ R_r(a) = \tau_{rrr}|_{r=a} = 0 \end{cases} \tag{a.12}$$

$$\begin{cases} T_r(b) = (\sigma^*_{rr} + \frac{1}{r}\tau_{r\theta\theta})\big|_{r=b} = -p_0 \\ R_r(b) = \tau_{rrr}|_{r=b} = 0 \end{cases} \tag{a.13}$$

For the axi-symmetric cavity expansion problem, the displacements u_r depend on r only. The strain gradients thus have the following non-zero components:

$$\eta_{rrr} = \frac{\partial^2 u_r}{\partial r^2}, \quad \eta_{\theta\theta r} = \frac{1}{r^2}\left(r\frac{\partial u_r}{\partial r} - u_r\right), \quad \eta_{r\theta\theta} = \eta_{\theta r\theta} = \frac{1}{r}\left(\frac{\partial u_r}{\partial r} - \frac{u_r}{2r}\right). \tag{a.14}$$

Appendix B. Cavity expansion solution using conventional theory

It is assumed that in the conventional theory, the elastic relations presented in Eq. (8) hold for the plane strain cavity expansion problem. In addition, the Tresca criterion is assumed to govern the yield behaviour in the cylinder:

$$\sigma_{\theta\theta} - \sigma_{rr} = \kappa. \tag{b.1}$$

where $\sigma_{\theta\theta}$ and σ_{rr} are the maximum and minimum principal stresses respectively.

The expansion pressure and the outer surface displacement are:

$$p = \kappa\left(\frac{b^2-\rho^2}{2b^2} + \ln\frac{\rho}{a}\right) + p_0. \tag{b.2}$$

$$u = \frac{\kappa\rho^2}{4b}\left(\frac{1}{\lambda+\mu} + \frac{1}{\mu}\right) - \frac{p_0 b}{2(\lambda+\mu)}. \tag{b.3}$$

while the stresses in the elastic and plastic regimes of the cylinder read:

$$\begin{cases} \sigma_{rr} = \kappa\ln\frac{r}{a} - p \\ \sigma_{\theta\theta} = \kappa\left(1+\ln\frac{r}{a}\right) - p \end{cases} \quad \textbf{Plastic regime } (a \leqslant r \leqslant \rho). \tag{b.4}$$

$$\begin{cases} \sigma_{rr} = 2(\lambda+\mu)A - \frac{2\mu}{r^2}B \\ \sigma_{\theta\theta} = 2(\lambda+\mu)A + \frac{2\mu}{r^2}B \end{cases} \quad \textbf{Elastic regime } (\rho < r \leqslant b) \tag{b.5}$$

where $A = \frac{(p-\kappa\ln\frac{\rho}{a})\rho^2 - p_0 b^2}{2(\lambda+\mu)(b^2-\rho^2)}$, $B = \frac{(p-p_0-\kappa\ln\frac{\rho}{a})\rho^2 b^2}{2\mu(b^2-\rho^2)}$.

Appendix C

C.1. Shooting procedure for elastic cavity expansion

(1) Enter with the parameters: a, b/a, λ/μ, c/μ, l/a, κ/μ, the specified tolerance TOL, the maximum number of iterations $MAXITS$, the perturbation tolerance $EPS_0 = \sqrt{eps}$ where eps denotes the machine precision, and the simple mixing coefficient for the update in the Broyden method χ.

(2) Enter with the pressure level at inner and outer walls of the cylinder: p^{int} and p^{out}.

(3) Enter the initial guess for y_1 and y_2 at $r = a$, respectively: $\xi^0 (= Aa + (B/a))$ and $\zeta^0 (= A - (B/a^2))$, and form the vector: $\mathbf{X}^0 = (\,\xi^0 \quad \zeta^0\,)^{\mathrm{T}}$.

(4) Substitute $\mathbf{X}^0 = (\,y_1 \quad y_2\,)^{\mathrm{T}} = (\,\xi^0 \quad \zeta^0\,)^{\mathrm{T}}$ into Eq. (16) to compute the initial value for y_3 and y_4 at $r = a$, which are denoted as y_3^0 and y_4^0.

(5) Use $\mathbf{Y}_a^0 = [\,\xi^0 \quad \zeta^0 \quad y_3^0 \quad y_4^0\,]^{\mathrm{T}}$ as the initial condition to solve the first order differential equation system Eq. (15) by a fourth-order explicit Runge–Kutta method. Obtain the solution for $\mathbf{Y}$ over $r = [a,b]$ and denote it as $\mathbf{Y}^1$.

(6) Extract the values of $\mathbf{Y}^1$ at $r = b$: $\mathbf{Y}_b^1 = [\,y_1^1(b) \quad y_2^1(b) \quad y_3^1(b) \quad y_4^1(b)\,]^{\mathrm{T}}$.

(7) Substitute $\mathbf{Y}_b^1$ into Eq. (17) to obtain the error vector $\mathbf{F}^0 = (\,f_T^0 \quad f_R^0\,)^{\mathrm{T}}$, where

$$\begin{cases} f_{\mathrm{T}}^0 = \frac{p_0}{\mu} + \left(-5\frac{c}{\mu}l^2 y_{4b} - \frac{6cl^2}{b\mu}y_{3b} + \left(\left(\frac{\lambda}{\mu}+2\right) + \frac{49cl^2}{4\mu b^2}\right)y_2 + \left(\frac{\lambda}{b\mu} - \frac{19cl^2}{2\mu b^3}\right)y_1\right) \\ f_{\mathrm{R}}^0 = \frac{c}{\mu}l^2\left(5y_{3b} + \frac{4}{b}y_{2b} - \frac{13}{4b^2}y_{1b}\right) \end{cases} \tag{c.1}$$

(8) Compute the square of the Euclidean norm of $\mathbf{F}^0$ as $|\mathbf{F}^0| = \sqrt{(f_{\mathrm{T}}^0)^2 + (f_{\mathrm{R}}^0)^2}$.

(9) If $|\mathbf{F}^0| \leqslant TOL$, go to step (24).

(10) Impose small perturbations to ξ^0 and ζ^0, according to $\delta\xi^0 = EPS_0 \times \xi^0$ and $\delta\zeta^0 = EPS_0 \times \zeta^0$, and let $\xi^{0\prime} = \xi^0 + \delta\xi^0$, $\zeta^{0\prime} = \zeta^0 + \delta\zeta^0$.

(11) Substitute $y_1 = \xi^{0\prime}$ and $y_2 = \zeta^0$ into Eq. (16) to compute a new vector $\mathbf{Y}_a^*$ at $r = a$. Use $\mathbf{Y}_a^*$ as the initial condition to solve the differential equation system Eq. (15) by the fourth-order explicit Runge–Kutta method, and obtain the solution for $\mathbf{Y}$ over $r = [a,b]$: $\mathbf{Y}^*$. Extract the values of $\mathbf{Y}$ at $r = b$: $\mathbf{Y}_b^*$.
(12) Substitute $y_1 = \xi^0$ and $y_2 = \zeta^{0\prime}$ into Eq. (16) to obtain another vector $\mathbf{Y}_a^+$. Use $\mathbf{Y}_a^+$ as the initial condition to solve the differential equation system of Eq. (15) by the fourth-order Runge–Kutta method, and obtain the solution for $\mathbf{Y}$ over $r = [a,b]$: $\mathbf{Y}^+$. Extract the values of $\mathbf{Y}^+$ at $r = b$: $\mathbf{Y}_b^+$.
(13) Substitute $\mathbf{Y}_b^*$ and $\mathbf{Y}_b^+$ into Eq. (c.1) to obtain $\mathbf{F}^* = (f_{\mathrm{T}}^* \quad f_{\mathrm{R}}^*)^{\mathrm{T}}$ and $\mathbf{F}^+ = (f_{\mathrm{T}}^+ \quad f_{\mathrm{R}}^+)^{\mathrm{T}}$, respectively.
(14) Compute:

$$\mathbf{A}^0 = \begin{bmatrix} \frac{(f_{\mathrm{T}}^* - f_{\mathrm{T}}^0)}{\delta\xi^0} & \frac{(f_{\mathrm{T}}^+ - f_{\mathrm{T}}^0)}{\delta\zeta^0} \\ \frac{(f_{\mathrm{R}}^* - f_{\mathrm{R}}^0)}{\delta\xi^0} & \frac{(f_{\mathrm{R}}^+ - f_{\mathrm{R}}^0)}{\delta\zeta^0} \end{bmatrix} \tag{c.2}$$

(15) Compute $\mathbf{B}^0 = (\mathbf{A}^0)^{-1}$ and set $\mathbf{s}^0 = -\mathbf{B}^0 \times \mathbf{F}^0$. Update $\mathbf{X}$: $\mathbf{X}^1 = \mathbf{X}^0 + \mathbf{s}^0$.
(16) Perform steps (17) to (22) *MAXITS* times:
(17) Use $\mathbf{X}^1 = (\xi^1 \quad \zeta^1)^{\mathrm{T}}$ and repeat steps (3) to (6) to obtain the new distribution of $\mathbf{Y}$ over $r = [a,b]$: $\mathbf{Y}^1$, and a new vector $\mathbf{F}^1 = (f_{\mathrm{T}}^1 \quad f_{\mathrm{R}}^1)^{\mathrm{T}}$. Compute $|\mathbf{F}^1|$ as in step (8).
(18) If $|\mathbf{F}^1| \leqslant TOL$, go to Step (24).
(19) Compute $\mathbf{B}^1$ using:

$$\mathbf{B}^1 = \mathbf{B}^0 + \frac{(\mathbf{s}^0 - \mathbf{B}^0(\mathbf{F}^1 - \mathbf{F}^0))(\mathbf{s}^0)^{\mathrm{T}}\mathbf{B}^0}{(\mathbf{s}^0)^{\mathrm{T}}\mathbf{B}^0(\mathbf{F}^1 - \mathbf{F}^0)} \tag{c.3}$$

(20) Compute $\mathbf{s}^1 = -\mathbf{B}^1 \times \mathbf{F}^1$. Then update: $\mathbf{X}^{1\prime} = \mathbf{X}^0 + \mathbf{s}^0$.
(21) Use simple mixing to update $\mathbf{X}$: $\mathbf{X}^1 = (1 - \chi)\mathbf{X}^1 + \chi\mathbf{X}^{1\prime}$.
(22) Set $\mathbf{F}^0 = \mathbf{F}^1$, $\mathbf{s}^0 = \mathbf{s}^1$, $\mathbf{B}^0 = \mathbf{B}^1$ and go to Step (14).
(23) Convergence not achieved after *MAXITS* iterations. Print error message and stop.
(24) Exit with $\mathbf{Y}^1$.

C.2. Load stepping procedure for elastic cavity expansion

(1) Enter with parameters: a, b/a, λ/μ, p_0/μ, $\Delta p/p_0$, c/μ, l/a, κ/μ, *TOL*, *MAXITS*, $EPS_0 = \sqrt{eps}$, χ.
(2) Increase the hydrostatic pressure from zero to p_0.
(3) Compute the displacement solution at p_0 using the above shooting procedure. Compute the corresponding stress field in the cylinder.
(4) For each point along the radius of the cylinder, compute the corresponding stresses $\sigma_{\theta\theta}^*$, σ_{rr}^* and σ_{zz}^*. Choose the maximum stress among the three as $\sigma_{\max}^*$ and the minimum one as $\sigma_{\min}^*$.
(5) If at any point, $\sigma_{\max}^* - \sigma_{\min}^* - \kappa > TOL$, the initial hydrostatic pressure p_0 is too large. Choose a smaller value for p_0 and repeat Steps (3) to (5).
(6) Let $p_1 = p_0$. Estimate p_{ci} by using Eq. (b.2) in Appendix B. Calculate $\Delta p_s = (p_{\mathrm{ci}} - p_0)/10$.
(7) Increase the inner cavity pressure by Δp_s from p_1 to p_2: $p_2 = p_1 + \Delta p_s$. Use the shooting procedure to compute the corresponding displacement and stress solutions.
(8) For each point along the radius of the cylinder, compute the stresses $\sigma_{\theta\theta}^*$, σ_{rr}^* and σ_{zz}^*. Choose the maximum stress among the three as $\sigma_{\max}^*$ and the minimum one as $\sigma_{\min}^*$. Compute the value of $K = (\sigma_{\max}^* - \sigma_{\min}^*)$ for each point.
(9) Of all the points along the cylinder radius, find two points where the value of K is the largest K_{m1} and next to largest K_{m2}, respectively.
(10) If $(K_{m1} - \kappa) < -TOL$, the cylinder is still in a purely elastic state. Set $p_2 = p_1$ and go to Step (7).
(11) If $|K_{m1} - \kappa| \leqslant TOL$ and $(K_{m2} - \kappa) < -TOL$, initial yielding occurs. Go to Step (13).
(12) If $(K_{m2} - \kappa) > TOL$, the initial yielding point has been overshot. Set $\Delta p_s = \Delta p_s/2$ and go to Step (7).
(13) Exit with p_2 and the corresponding displacement and stress solutions.

C.3. Procedure for the plastic solution of gradient-dependent cavity expansion

(1) Enter with the following parameters: a, b/a, λ/μ, c/μ, l/a, κ/μ, χ, TOL, $MAXITS$, $EPS_0 = \sqrt{eps}$.
(2) Enter the total number of increments for ρ stepping from a to b: N_ρ.
(3) Compute: $\Delta\rho = (b-a)/N_\rho$.
(4) Use the numerical shooting procedure to solve the two-point boundary value problem constituted by Eqs. (15), (19) and (17), and find the displacements and their gradients across the cylinder on initial yielding $\mathbf{Y}_{yi}$.
(5) Use $\mathbf{Y}_{yi}$ to compute the stresses and higher stresses at $\rho_0 = a$, and substitute these stresses into Eq. (20) to evaluate the critical cavity pressure at initial yielding. Compute $\hat{\tau}^{(a)}_{r\theta\theta}$.
(6) Evaluate φ_0 by Eq. (25) and $\mathbf{Y}_{yi}$ at $\rho_0 = a$. Set $\tilde{\varphi}_0 = \varphi_0$.
(7) Increment ρ_0 by $\Delta\rho$: $\rho_1 = \rho_0 + \Delta\rho$.
(8) Let $dy_4/dr = \tilde{\varphi}_0$ in Eq. (24). Solve Eqs. (15), (24) and (17) using the numerical shooting method, and obtain the displacement vector $\mathbf{Y}$ for $\rho_1 \leqslant r \leqslant b$.
(9) Compute $\tilde{\varphi}_1$ according to Eq. (26) using $\mathbf{Y}$ at $r = \rho_1$. Calculate $\delta = |\tilde{\varphi}_1 - \tilde{\varphi}_0|/|\tilde{\varphi}_0|$.
(10) If $\delta > TOL$, let $\tilde{\varphi}_0 = \tilde{\varphi}_1$. If $\delta \leqslant TOL$, go to Step (12).
(11) If $\rho_1 < b$, go to Step (8). If $\rho_1 = b$, go to Step (9).
(12) Save $\mathbf{Y}$, compute the stress field for $\rho_1 \leqslant r \leqslant b$; Compute the stresses and current cavity pressure according to Eqs. (28) and (30).
(13) Set $\tilde{\varphi}_0 = \tilde{\varphi}_1$. If $\rho_1 < b$, go to Step (7). If $\rho_1 = b$, go to Step (14).
(14) Exit with the obtained solutions to the plastic cavity expansion.

References

Burland, J.B., Rampello, S., Georgiannou, V.N., Calabresi, G., 1996. A laboratory study of the strength of four stiff clays. Géotechnique 46 (3), 491–514.

Carter, J.P., Booker, J.R., Yeung, S.K., 1986. Cavity expansion in cohesive frictional soils. Géotechnique 36 (3), 349–353.

Chambon, R., Caillerie, D., El Hassan, N., 1998. One-dimensional localisation studied with a second grade model. European Journal of Mechanics – A/Solids 17 (4), 637–656.

Chambon, R., Caillerie, D., Tamagnini, C., 2004. A strain space gradient plasticity theory for finite strain. Computer Methods and Application in Mechanical Engineering 193, 2797–2826.

Chambon, R., Moullet, J.C., 2004. Uniqueness studies in boundary value problems involving some second gradient models. Computer Methods and Application in Mechanical Engineering 193, 2771–2796.

Chambon, R., Caillerie, D., Matsuchima, T., 2001. Plastic continuum with microstructure, local second gradient theories for geomaterials: localization studies. International Journal of Solids and Structures 38, 8503–8527.

Collins, I.F., Pender, M., Wang, Y., 1992. Cavity expansion in sands under drained loading conditions. International Journal for Numerical and Analytical Methods in Geomechanics 16 (1), 3–23.

Cosserat, E., Cosserat, F., 1909. Théorie des Corps Déformables. Hermann A. et Files, Paris.

Eringen, A.C., 1967. Mechanics of Continua. John Wiley.

Fleck, N.A., Hutchinson, J.W., 1993. A phenomenological theory for strain gradient effects in plasticity. Journal of the Mechanics and Physics of Solids 41 (12), 1825–1857.

Fleck, N.A., Hutchinson, J.W., 1997. Strain gradient plasticity. In: Hutchinson, J.W., Wu, T.Y. (Eds.), Advances in Applied Mechanics, vol. 33. Academic Press, New York, pp. 295–361.

Germain, P., 1973. The method of virtual power in continuum mechanics. Part 2 Microstructure. SIAM Journal of Applied Mathematics 25, 556–575.

Gibson, R.E., Anderson, W.F., 1961. In situ measurement of soil properties with the pressuremeter. Civil Engineering and Public Works Reviews 56, 615–618.

Hill, R., 1950. The Mathematical Theory of Plasticity. Oxford University Press, London.

Keller, H.B., 1968. Numerical Methods for Two-Point Boundary-Value Problems. Blaisdell, Waltham, MA, London.

Ladanyi, B., Foriero, A., 1998. A numerical solution of cavity expansion problem in sand based directly on experimental stress-strain curves. Canadian Geotechnical Journal 35, 541–559.

Mindlin, R.D., 1964. Micro-structure in linear elasticity. Archives for Rational Mechanics and Analysis 16, 51–78.

Mindlin, R.D., 1965. Second gradient of strain and surface tension in linear elasticity. International Journal for Solids and Structures 28, 845–857.

Salgado, R., Mitchell, J.K., Jamiolkowski, M., 1997. Cavity expansion and penetration resistance in sand. Journal of Geotechniques and Geoenvironmental Engineering, ASCE 123 (4), 344–354.

Stoer, J., Bulirsch, R., 1980. Introduction to Numerical Analysis. Springer-Verlag, New York.
Toupin, R.A., 1962. Elastic materials with couple stresses. Archives for Rational Mechanics and Analysis 11, 385–414.
Yu, H.S., Houlsby, G.T., 1991. Finite cavity expansion in dilatant soils: loading analysis. Géotechnique 41 (2), 173–183.
Yu, H.S., 1992. Expansion of a thick cylinder of soils. Computers and Geotechnics 14, 21–41.
Yu, H.S., 2000. Cavity Expansion Methods in Geomechanics. Kluwer Academic Publisher.
Zhao, J.D., Sheng, D.C., Zhou, W.Y., 2005. Shear banding analysis of geomaterials by strain gradient enhanced damage model. International Journal of Solids and Structures 42 (20), 5335–5355.
Zhao, J.D., Sheng, D.C., 2006. Strain gradient elasticity in orthogonal curvilinear coordinates. Mechanics Research Communication (under review).
Zhao, J.D., Sheng, D.C., Sloan, S.W., Krabbenhoft, K., 2007. Limit theorems for gradient-dependent elastoplastic geomaterials. International Journal of Solids and Structures 44 (2), 480–506.